Universidade de Brasília
Programa de Pós-graduação em Estruturas e Construção Civil
Departamento de Engenharia Civil e Ambiental

Spherical Harmonics on constitutive equations for biological cells

María Paz Duque Gutiérrez

Dissertação apresentada como requisito parcial para
conclusão do Doutorado em Estruturas e Construção Civil

Orientador
Prof. Dr. William Taylor Matias Silva

Brasília
2019

UNIVERSIDADE DE BRASÍLIA
FACULDADE DE TECNOLOGIA
DEPARTAMENTO DE ENGENHARIA CIVIL E AMBIENTAL

SPHERICAL HARMONICS ON CONSTITUTIVE EQUATIONS FOR BIOLOGICAL CELLS

MARÍA PAZ DUQUE GUTIÉRREZ

TESE DE DOUTORADO SUBMETIDA AO DEPARTAMENTO DE ENGENHARIA CIVIL E AMBIENTAL DA FACULDADE DE TECNOLOGIA DA UNIVERSIDADE DE BRASÍLIA COMO PARTE DOS REQUISITOS NECESSÁRIOS PARA A OBTENÇÃO DO GRAU DE DOUTOR EM ESTRUTURAS E CONSTRUÇÃO CIVIL.

APROVADA POR:

_____
Prof. William Taylor Matias Silva, Dr. Ing. (PECC-UnB)
(Orientador)

_____
Prof. Artur Antônio de Almeida Portela, PhD (PECC-UnB)
(Examinador Interno)

_____
Prof. Márcio Muniz de Farias, PhD (PPG-UnB)
(Examinador Externo)

_____
Prof. Zenón José Guzmán Nuñez Del Prado, PhD (UFG)
(Examinador Externo)

BRASÍLIA, 18 DE MARÇO DE 2019

To my parents

Acknowledgments

I would like to address my thanks to Prof. Dr. William Taylor Matias Silva for his constant support. During his years as my advisor, he has always been willing to address my doubts and provide me with a broad overview of the topics under discussion.

Many thanks to Dr. Mettupalayam Sivaselvan for allowing me to be part of the research project and for the valuable teachings conveyed during my stay at the University at Buffalo in the United States of America. Thanks also to UB doctoral student Ali Gurbuz.

Furthermore, I would like to thank the professors of the Postgraduate Program in Structures and Civil Construction of the University of Brasilia, who contributed a lot to my learning.

Additional thanks go to the CNPQ and to the PhD exchange program from CAPES for providing financial support.

I would also like to thank the following people:

Óscar, Mirian, Natalia, Daniela, Emma, Mila, Sebastián, Sara, Rosalba and Isabel. You are everything to me; every day I am thankful for being part of a family full of love and understanding. Many thanks to my family and friends in Colombia, who are always present in my life.

To my dear friends in Brasília, Armando, Vanessa, Dulce, Helard, Yina, Carlos, Julian, Eduardo, Sebastião, Marília, Luis Carlos, Wilson, Nathaly, Daniela, Juliana, Erwin, Diana, Carolina, Estefa, Rosa and my girls from home. I've never felt alone in Brazil, and I owe it to you.

To my friends and colleagues from PECC who were present in any capacity during the time of my research. We learned the importance of the long conversations and pleasant

moments that softened our sometimes difficult days as graduate students.

Finally, I want to thank the wonderful people I met in Buffalo, Jamil, Claudia and Mriganka. Your company was of great importance to me during the time I spent in the United States.

Resumo

Desenvolvem-se e avaliam-se neste trabalho modelos constitutivos não-lineares incluindo o estudo de grandes deformações com o objetivo de modelar células biológicas representadas por elementos de cascas finas. É utilizada como ponto de partida a formulação clássica de elementos de cascas finas, considerando as hipóteses de Kirchhoff que apresentam como mais importante característica a redução dimensional. Esta é atingida derivando tensões 2D como médias das tensões 3D pela integração direta sob a espessura da casca. Para a definição da deformação do continuo é utilizada uma descrição Lagrangiana. As células biológicas não podem ser modeladas de forma correta utilizando modelos constitutivos lineares. Especificamente no estudo dos glóbulos vermelhos devem ser considerados: o comportamento elástico não linear e o aporte da viscosidade da parede da célula. Consequentemente, neste trabalho, modelos hiperelasticos são implementados junto ao modelo de Kelvin-Voigth para obter um modelo viscoelástico. Na implementação computacional Funções de Esféricos Harmônicos são utilizadas para sintetizar as principais variáveis, esforços e deslocamentos. Isto se deve a que a geometria dos glóbulos vermelhos pode ser descrita de forma simples utilizando coordenadas esféricas. Resultando numa implementação de baixo custo computacional que consegue lidar com altas não linearidades.

Este trabalho apresenta uma formulação de um método indireto pois consiste no cálculo de coeficientes da expansão de Esféricos Harmônicos, sendo que estes coeficientes não têm sentido físico. É importante mencionar que o projeto se encontra num estágio inicial e não foi encontrado na literatura uma aplicação utilizando teoria de cascas, Harmônicos Esféricos junto com modelos constitutivos lidando com grandes deformações. Finalmente o método é validado e estudado suas possíveis aplicações.

Palavras-chave: Glóbulos Vermelhos, Relações Constitutivas, Harmônicos Esféricos

Abstract

In this work, constitutive models are developed and evaluated with the aim of modeling biological cells represented by thin shell elements in a second-order analysis. The classical formulation of thin shell elements is used while considering dimensional reduction, which is the main feature of the Kirchhoff hypotheses. This reduction is achieved by deriving two-dimensional stresses as averages of the true three-dimensional stresses by means of direct integration through the shell thickness. A Lagrangian description is used to define the deformation of the continuum. Biological cells cannot be correctly modeled using linear constitutive relations. Specifically, in the study of red blood cells, one should consider both their nonlinear elastic behavior and the contribution of the cell wall viscosity. Consequently, hyperelastic constitutive equations are implemented using the Kelvin-Voigt approach to obtain a viscoelastic model. In the computational implementation, spherical harmonic functions are used to synthesize the main variables, resultant forces and displacements since the geometry of red blood cells can be simply described using spherical coordinates. As a result, a low-cost computational implementation for highly nonlinear analyses is obtained. This work presents a formulation of an indirect method since consists on the calculation of the expansion coefficients of a Spherical Harmonic Analysis, these coefficients have no physical meaning. It is important to mention that this work is part of a project that is at an early stage. In the literature no application was found using shell theory, Spherical Harmonics with constitutive models dealing with large deformations. Finally, the method is validated and its possible applications are discussed.

Keywords: Red Blood Cells, Contitutive Relations, Spherical Harmonics

FICHA CATALOGRÁFICA

DUQUE GUTIÉRREZ, MARÍA PAZ
Spherical Harmonics on constitutive equations for biological cells. [Distrito Federal] 2019.
x, 74p., 297 mm (ENC/FT/UnB, Doutora, Estruturas e Construção Civil, 2019).
Tese de Doutorado - Universidade de Brasília. Faculdade de Tecnologia.
Departamento de Engenharia Civil e Ambiental.
1. Glóbulos vermelhos 2. Relações constitutivas
3. Harmônicos esféricos
I. ENC/FT/UnB II. Título (série)

REFERÊNCIA BIBLIOGRÁFICA

GUTIERREZ, M. P. D. (2019). Spherical Harmonics on constitutive equations for biological cells. Tese de Doutorado em Estruturas e Construção Civil. Publicação E.TD-5A/19, Departamento de Engenharia Civil e Ambiental, Universidade de Brasília, Brasília, DF, 74p.

CESSÃO DE DIREITOS

AUTOR: María Paz Duque Gutiérrez

TÍTULO: Spherical Harmonics on constitutive equations for biological cells.

GRAU: Doutora ANO: 2019

_____

María Paz Duque Gutiérrez
SQN 406, Bloco K apto 204 - Asa Norte
70.847-110 Brasília - DF- Brasil
e-mail: mpazduque@gmail.com

Nomenclature

$(\cdot)_\alpha$	$(\cdot)$ in surface coordinates, $\alpha = 1, 2$
$(\cdot)_i$	$(\cdot)$ in ambient coordinates, $i = 1, 2, 3$
δ^i_j	Kronecker delta
$\epsilon_{\alpha\beta}$	strain tensor
$\kappa_{\alpha\beta}$	bending tensor
σ	true stress tensor
$\mathbf{a}^\alpha$	contravariant basis of the middle surface
$\mathbf{a}_\alpha$	covariant basis of the middle surface
$\mathbf{C}$	right Cauchy-Green tensor
$\mathbf{E}$	Green-Lagrange strain tensor
$\mathbf{e}$	strain rate tensor
$\mathbf{F}$	deformation gradient
$\mathbf{g}^i$	contravariant basis of a point in the shell continuum
$\mathbf{g}_i$	covariant basis of a point in the shell continuum
$\mathbf{n}$	normal vector to a surface
$\mathbf{r}$	position vector
$\mathbf{S}$	second Piola-Kirchhoff stress tensor
$\mathbf{S}^\alpha$	contravariant basis of a surface
$\mathbf{S}_\alpha$	covariant basis of a surface

$\mathbf{v}$	velocity field
$\mathbf{Z}^i$	contravariant basis
$\mathbf{Z}_i$	covariant basis
μ^s	surface viscosity
∇_α	covariant derivative
Ψ	strain-energy function
$a^{\alpha\beta}$	contravariant metric tensor of the middle surface
a^α	coordinates of the middle surface
$a_{\alpha\beta}$	covariant metric tensor of the middle surface
$a_{m,n}, b_{m,n}$	coefficients of the spherical harmonics function
$b_{\alpha\beta}$	second fundamental tensor of the middle surface
g^{ij}	contravariant metric tensor of a point in the shell continuum
g_{ij}	covariant metric tensor of a point in the shell continuum
h	shell thickness
I_i	invariants of a matrix
$m^{\alpha\beta}$	bending stress tensor
$n^{\alpha\beta}$	membrane stress tensor
p^i	resultant force on a shell
q^α	shear force vector
u^α	surface coordinates
x^i	Cartesian coordinates
Z_i^α	shift tensor
Z^{ij}	contravariant metric tensor
Z_{ij}	covariant metric tensor

Contents

1 Introduction **1**

1.1 Objectives 4

1.2 Document structure 4

2 Literature Review **6**

2.1 Modeling of RBCs 6

2.2 Constitutive behavior of RBCs 8

2.3 Harmonic analysis approach 9

2.3.1 Spherical harmonics research in "Web of Science" 10

3 Shell Theory **23**

3.1 Basic notions of tensor calculus 23

3.2 The geometry of the middle surface 26

3.3 Shell continuum 27

3.4 Kinematics 28

4 Constitutive Relations **31**

4.1 Hyperelastic model 31

4.1.1 Strain-energy functions 34

4.2 Membrane viscosity 35

4.3 Statics of a shell 37

5 Numerical Technique: Spherical Harmonics Functions **38**

5.1 Spectral methods 38

5.2 Spherical harmonics 39

5.3 Implementation of the harmonic analysis 43

6 Numerical applications **45**

6.1 Spherical balloon 45

6.2 RBC simulations in an infinite shear flow 51

7 Conclusions **62**
7.1 General conclusions 62
7.2 Future Works 64

Bibliography **65**

Annex **72**

I Surface properties: Sphere **73**

List of Figures

1.1 Sketch of a RBC 3

2.1 Keywords for spherical harmonics in Civil Engineering. Original image from VOSviewer 11
2.2 Result Analysis for authors for spherical harmonics in Civil Engineering. Original image from web of science 12
2.3 Citation report for spherical harmonics in Civil Engineering. Original image from web of science 12
2.4 Keywords for spherical harmonics in Engineering Biomedical. Original image from VOSviewer 13
2.5 Result Analysis for authors for spherical harmonics in Engineering Biomedical. Original image from web of science 14
2.6 Citation report for spherical harmonics in Engineering Biomedical. Original image from web of science 15
2.7 Keywords for spherical harmonics in Applied Mathematics. Original image from VOSviewer 16
2.8 Result Analysis for authors for spherical harmonics in Applied Mathematics. Original image from web of science 17
2.9 Citation report for spherical harmonics in Applied Mathematics. Original image from web of science 18
2.10 Keywords for spherical harmonics in Mechanical Engineering. Original image from VOSviewer 18
2.11 Result Analysis for authors for spherical harmonics in Mechanical Engineering 19
2.12 Citation report for spherical harmonics in Mechanical Engineering . Original image from web of science 20
2.13 Keywords for spherical harmonics in Mechanics. Original image from VOSviewer 20
2.14 Result Analysis for authors for spherical harmonics in Mechanics. Original image from web of science 21

2.15 Citation report for spherical harmonics in Mechanics. Original image from web of science 22

3.1 Representation of the middle surface 24

4.1 Spring-dashpot models. a) Maxwell b)Kelvin-Voigth. Lakes (2009) 35

5.1 Gauss points distribution 41
5.2 Gauss points of a 10 radius sphere 43

6.1 Internal pressure p 46
6.2 Inflation of a balloon: stretch-pressure curve 47
6.3 Inflation of a balloon: stretch-pressure curve 48
6.4 Inflation of a balloon: undeformed and deformed geometries 48
6.5 Inflation of a balloon: stretch-stress curve 49
6.6 Inflation of a balloon: stretch-stress curve 50
6.7 Inflation of a balloon: stretch-stress curves varying nlat 50
6.8 Undeformed RBC 52
6.9 Sketch of an undeformed RBC 52
6.10 Sketch of an undeformed RBC suspended in a simple shear flow 53
6.11 From Pozrikidis (2005). A suspension of human RBCs moving through glass tubes with approximate diameters 4.5 μm (top), 7 μm (middle), and 15 μm (bottom); the flow direction is from left to right. 54
6.12 Snapshots of a RBC in a simple shear flow 54
6.13 Snapshots of a RBC in a simple shear flow 55
6.14 Resultant traction vs. Stretch for the viscoelastic and hyperelastic models . 55
6.15 Position of the Gauss points for the resting RBC 56
6.16 Snapshot of a RBC in a simple shear flow. $step = 1$ 56
6.17 Snapshot of a RBC in a simple shear flow. $step = 1000$ 57
6.18 Snapshot of a RBC in a simple shear flow. $step = 2000$ 57
6.19 Snapshot of a RBC in a simple shear flow. $step = 3000$ 58
6.20 Snapshot of a RBC in a simple shear flow. $step = 4000$ 58
6.21 Snapshot of a RBC in a simple shear flow. $step = 5000$ 59
6.22 Snapshot of a RBC in a simple shear flow. $step = 6000$ 59
6.23 Snapshot of a RBC in a simple shear flow. $step = 7000$ 60
6.24 Snapshot of a RBC in a simple shear flow. $step = 8000$ 60
6.25 Snapshot of a RBC in a simple shear flow. $step = 9000$ 61
6.26 Snapshot of a RBC in a simple shear flow. $step = 10000$ 61

Chapter 1

Introduction

The main goal of engineering research is to develop tools for analyzing various complex problems. With the continuing advance of new digital technologies, all kinds of research are entering a new era that is rapidly evolving.

For nonlinear analysis, the finite element method (FEM) has enabled the treatment of a wide range of structural problems in civil, aerospace, and aeronautic engineering as well as other fields. Nonetheless, for some problems, some of which are highly complex, other numerical methods must be applied to avoid numerical instabilities that will prevent the problem from being solved or to lower the computational cost.

In the past two decades, applications involving biological materials such as bones (Eremeyev *et al.*, 2017), muscles (Karami and Eghtesad, 2018), and arteries (Dolgov *et al.*, 2019) have been thoroughly studied based on fundamental concepts of continuum mechanics, and such applications have emerged as an important field of study.

The boundary element method (BEM), the smoothed particle hydrodynamics (SPH) method and the FEM itself have all been implemented for problems of this type, resulting in important contributions.

This work was performed as part of a research project led by Dr. Mettupalayam Sivaselvan, Associate Professor in the Department of Civil, Structural and Environmental Engineering at the University at Buffalo, with the aim of simulating the behavior of red blood cells (RBCs) passing through microcapillaries. Specifically, this work focused on modeling the shell mechanics of the RBC membrane.

Blood is a fluid connective tissue that circulates through the cardiovascular system which consists of a suspension of various elements (erythrocytes, leukocytes, and platelets) in plasma. Total blood volume in the average adult is about 6 L or 7% to 8% of total body weight. The functions of the blood are: to transport nutrients, oxygen, wastes and carbon dioxide to and from the tissues; to convert hormones, cytokines, chemokines and other solubleregulatory molecules; and to transport leukocytes and antibodies through the tissues Ross and Pawlina (2011).

The volume of the erythrocytes (RBCs) in a sample of blood is called the hematocrit. The hematocrit is typically approximately 45% of the total blood volume. The viscosity of blood is directly related to the number of RBCs. Hence, understanding the behavior of the RBCs is very important.

RBC are anucleate cells devoid of typical organelles. The function of red blood cells (RBCs) is to carry haemoglobin around the body in high concentrations such that oxygen is taken up in the lungs and delivered to the tissue Gordon-Smith (2007). Their shape is a biconcave disk, $8\mu m$ diameter, $2\mu m$ at thickest point, $1\mu m$ at thinnest maintained by a cytoskeletal complex inside the plasma membrane (involving spectrin, actin and other components) as shown in Figure 1.1. The life span of erythrocytes is approximately 120 days.

RBC are extremely flexible cells which normally bend to pass through small capillaries. They pass easily through the narrowest capillaries by folding over on themselves. They stain uniformly with eosin. The shape of the erythrocyte is maintained by membrane proteins. The cell membrane of an erythrocyte is composed of a typical lipid bilayer and contains two functionally significant groups of proteins:

- Integral membrane proteins represent most of the proteins in the lipid bilayer
- Peripheral membrane proteins reside on the inner surface of the cell membrane. They are organized into a two-dimensional hexagonal lattice network that laminates the inner layer of the membrane.

. Consequently, simulations of this behavior might be very useful in the study of blood flow, its properties and membrane characterization. In combination with laboratory monitoring, this could be beneficial for the diagnosis of diseases such as anemia, malaria and diabetes.

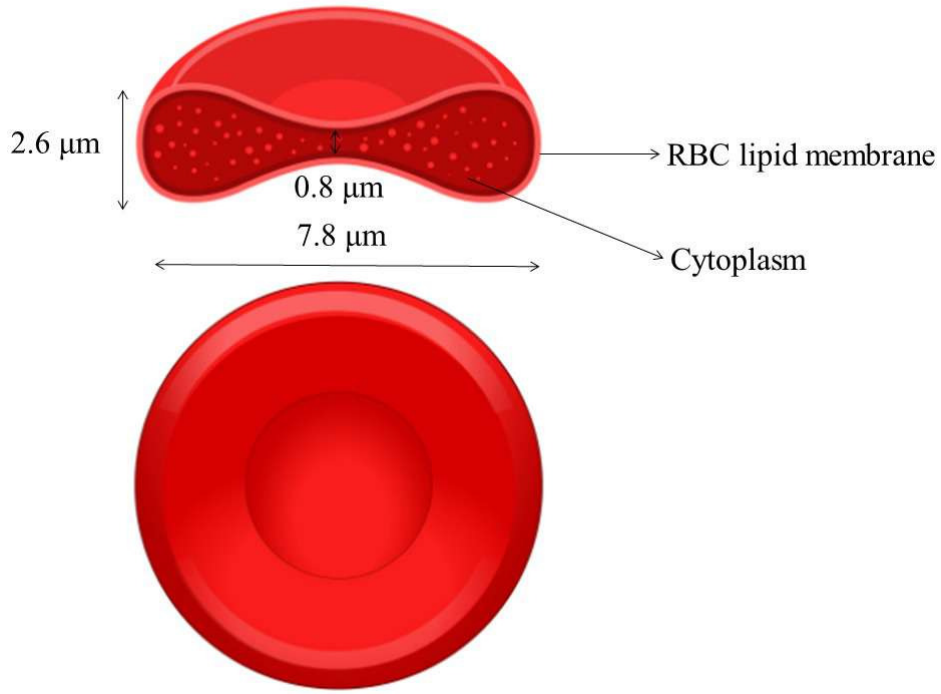

Figure 1.1: Sketch of a RBC

Since the cross-sectional area of a microscale capillary vessel can often be smaller than the diameter of an RBC, RBCs typically undergo significant structural deformation to pass through such vessels (Meyers *et al.*, 2008). Therefore, the cells respond to external stimuli, changing their shape or mechanical properties, which could lead to membrane damage under extreme conditions. This work does not address biological or chemical processes inside the cell but rather focuses on the whole-cell scale.

Due to changes in its composition (caused by lack of proteins, aging of the cells, etc.), the RBC membranes lose their ability to deform and show a more rigid behavior, hindering passage through the capillaries. The research group led by Dr. Mettupalayam Sivaselvan is proposing a new methodology for leading with the numerical implementation of the RBC membrane behavior.

The research group is introducing the use of spherical harmonics for a numerical treatment of the problem. Spherical harmonics are a natural basis for representing functions defined over spherical and hemispherical domains. Swarztrauber (1993) presented a method of solving either steady or time-dependent partial differential equations expressed in spherical coordinates. This introduced the harmonic transform solution method, which belongs to the category of spectral transform methods.

The code developed by Dr. Sivaselvan group it's written in Matlab and serves as a tool to obtain the stresses of a shell element using a spherical harmonics technique by means of a Fortran routines for the calculation of the variables needed in this particular application.

As a novel contribution, this work studied and implemented the nonlinear constitutive behavior of the RBC membrane using the spherical harmonics technique. As a result, a compact and low-cost code for modeling RBCs is developed. Taking advantage of the fact that the geometry of an RBC can be expressed in spherical coordinates, spherical harmonic functions can be used to express the variables of the problem (such as, stresses and strains) in a global manner. It is important to note that the project is still in its early stages.

1.1 Objectives

General Objective

To model the shell mechanics of the Red Blood Cells membrane which can be applied in the simulation of RBC behaviour passing through microcapillaries.

Specific Objectives

- To study the nonlinear behaviour of RBC and the numerical methods used in its modelling.
- To study the kinematics assumptions of the shell theory necessary to the simulation of RBC membrane.
- To implement the spherical harmonics technique on modelling RBC membrane.
- To evaluate the implementation of spherical harmonics using a validation example and comparing with analytical and numerical results.

1.2 Document structure

The outline of this work is as follows.

- Chapter 2 a brief review of the literature is presented below. A few works are mentioned in which the study of nonlinear RBC and capsule behavior was treated. It is shown that various numerical methods have been applied.

- Chapter 3 contains a general overview of the relevant shell theory, which serves as the basis of this work. Some essential kinematics concepts and the fundamentals of structural mechanics are presented.

- In Chapter 4, the nonlinear constitutive equations used for the modeling of RBCs are formulated. First, hyperelastic models and some strain-energy functions are described. Then, the Kelvin-Voigt model is applied.

- The spherical harmonics technique is studied in Chapter 5. The SPHEREPACK suite, which is used in the computations of the nonlinear response of the shell continuum, is introduced.

- A validation example is presented in Chapter 6, for which analytical and numerical results are shown and compared. Simulations of an RBC in an infinite shear flow are discussed.

- The final chapter gives a summary of the conclusions and outlooks. Ideas for future research are proposed.

Chapter 2

Literature Review

For the development of this research some important topics were studied prior to the implementation of the RBCs membrane model. Initially, we investigated the different approaches on modeling RBCs membrane, where shell elements have been predominantly used for numerical applications. In regards to the mechanical model, the cell was treated as comprising material with certain continuum material properties. In order to define the constitutive behavior of RBCs, some researches were explored, including MEF approaches.

The following are the main articles related to the topics of: Modeling of RBCs, constitutive behavior of RBCs and finally Harmonic analysis approach.

2.1 Modeling of RBCs

In the modeling of biological membranes as RBCs, shell elements have been predominantly used for numerical implementations. 3D elements in which one dimension is considerably smaller than the other two are known as shells. These elements have a wide range of applications in structural mechanics.

Dimensional reduction lies at the core of shell theory and is usually achieved by replacing dependent variables, such as deformations and stresses, with their averages or weighted averages calculated over the thickness of the shell (Niordson, 1985). These structural elements have many useful properties; even thin shells can support large loads. Therefore, shells are utilized in structures in which a light weight is essential.

There have been several publications on the modeling of biological cells. Lim *et al.* (2006) presents a review of several mechanical models used for the study of living cells. For example, Rand and Burton (1964) can be highlighted as the first study in which the

micropipette aspiration technique was used to measure the mechanical properties of the RBC membrane, whereas the optical tweezers method was used in Hénon *et al.* (1999), Dao *et al.* (2003), Lim *et al.* (2004) and Mills *et al.* (2004).

The mechanical modeling approaches used for living cells can be divided into two categories. The micro-nanostructural approach focuses on the cytoskeleton. The cytoskeleton is a stable and dynamic network of protein fibers that gives a cell its shape and structure; it is the main structural component of the cell. An study of the cytoskeleton is presented in Satcher and Dewey (1996). In the continuum approach, the cell is treated as comprising materials with certain continuum material properties. This work falls into this category. The use of viscoelastic models has been well documented in the continuum approach. Such models can be divided into solid models and liquid drop models.

Liquid drop models are based on the fact that many cells exhibit liquid-like responses. The Newtonian liquid drop model and the Maxwell liquid drop model belong to this category (Lim *et al.*, 2006). White blood cells (Evans and Yeung, 1989) and eukaryotic cells (Dong *et al.*, 1991), among others, have been studied using liquid drop models.

In solid models, the cell is usually assumed to consist of a homogeneous material, either an incompressible elastic solid or a viscoelastic solid. An elastic model is a simplification of a viscoelastic model in which the time factor is neglected.

Unfortunately, a linear elastic model is usually not adequate to describe the mechanics of living cells. This is because the elastic part of a viscoelastic material will depend on its loading rate and loading history. In Mijailovich *et al.* (2002), an FEM model was implemented for magnetic twisting cytometry (MTC) considering a homogeneous, incompressible, linear elastic material.

Schmid-Schönbein *et al.* (1981) proposed a viscoelastic model for studying the small-strain deformation of human leukocytes, which was later modified in Sato *et al.* (1990), Cheng *et al.* (2000) and Koay *et al.* (2003) using several types of functions for creep compliance.

2.2 Constitutive behavior of RBCs

It has been shown that an RBC behaves as a two-dimensional, anisotropic material that is isotropic in the plane of the membrane. Stresses in the plane of the membrane are not coupled to the direction normal to the surface. Thus, the membrane cannot change thickness in response to an in-plane stress; therefore, applied forces are considered to be distributed in a per-unit-length manner (Evans and Hochmuth, 1976).

Coulumb The first studies of nonlinear elastic materials were Mooney (1940) and Rivlin and Rideal (1948). In these works, the theory of large elastic deformation was introduced based on the concept of a stored energy function for the derivation of the stress-strain relations. Rubber-like materials were the principal target of studies using such hyperelastic models.

Recently, these models have been applied in the modeling of RBCs. In Chee *et al.* (2008), using the commercially available finite element code ADINA, a three-dimensional fluid–structure interaction model of an RBC was presented that consists of a deformable liquid capsule modeled as a Newtonian fluid enclosed by a hyperelastic membrane with viscoelastic properties.

Also using an FEM code, Doddi and Bagchi (2008) modeled the motion of a deformable capsule undergoing large deformation following a neo-Hookean law. The membrane was discretized using flat triangular elements. In Peng *et al.* (2011), a computational model was developed by coupling a multiscale approach to the RBC membrane with a boundary element method for the surrounding Stokes flows, and the membrane was modeled using FEM; thus, an algorithm for coupling both methods was needed.

Yoon and You (2016) presented a study of the nonlinear elasticity of an RBC using the Yeoh hyperelastic material model in a framework of continuum mechanics based on a finite element approximation. Casquero *et al.* (2017) used a nonuniform rational B-splines (NURBS)-based approach to study the behavior of hyperelastic capsules in shear and parabolic flows.

Soleimani *et al.* (2018) developed a 3D numerical method for simulating RBCs based purely on the SPH method, in which the membrane was treated as a nonlinear deformable elastic shell, using several numerical remedies for the implementation instabilities.

In regards to membrane viscosity, the first related work was presented in Barthes-Biesel and Sgaier (1985). Until that time, all models had considered only cells surrounded by purely elastic sheets, inconsistent with numerous experimental studies showing that the membrane of an RBC exhibits a measurable viscosity (Evans and Hochmuth, 1976), for example. The authors of that study assessed the importance of the viscoelastic properties of the membrane by means of a regular perturbation analysis for the case in which the deformation is small.

After that, most numerical studies ignored the role of the membrane viscosity in the case of large deformations. Diaz *et al.* (2001) extended the study to capsules with hyperelastic membranes to account for the membrane viscosity. Yazdani and Bagchi (2013) presented a numerical method for the large deformation of capsules using a Kevin-Voigt viscoelastic model of the membrane; this is the same model used in this work. They noted wrinkles appearing in the cell membrane in a shear flow at a moderate rate, similar to those reported in experimental measurements.

Tang *et al.* (2017) presented a particle model for extracting RBC properties. However, it is computationally demanding, if not prohibitive, to simulate the large number of particles required for modeling the membrane of an entire RBC.

2.3 Harmonic analysis approach

Harmonic analysis has been applied in several relevant interdisciplinary areas, including signal and image processing, learning theory, big data analysis, and data recovery. As a numerical technique, a harmonic analysis was performed in this work based on spherical harmonic functions.

Spherical harmonic functions have been extensively studied and applied to solve a wide range of problems in mathematical science with the aim of solving problems involving partial differential equations on a unit sphere. In the same way that Fourier transforms are used on a rectangle in Cartesian coordinates, harmonic transforms are used on a sphere, with Fourier transforms being used in the longitudinal direction and Legendre transforms being used in the latitudinal direction.

Recent contributions in engineering such as Erdoğan (2016), several approaches involving computed tomography and spherical harmonic analysis have been compared in terms of their success in estimating the surface areas of micrometer-sized to centimeter-sized

particles. Kozłowski *et al.* (2018) proposed a solution for water consumption forecasting in a water supply system, wherein hourly water consumption is determined through trend analysis and harmonic analysis.

In Cheng and Shi (2018), the authors introduced a novel multidimensional composite periodic foundation for seismic isolation, for which harmonic analysis and time-history analysis results showed that the proposed foundation can effectively reduce the vibrations of the upper structure in both the horizontal and vertical directions.

Sarkar *et al.* (2018) proposed the use of machine learning techniques for the prediction of tidal currents using kernel functions to capture structures in the data. Han and Cao (2018) implemented a numerical model for the drainage and deformation of intercalated confining layers due to internal stress changes (the discharge/recharge cycle) in an aquifer-aquitard system with the help of harmonic analysis.

To the best of the author's knowledge, there has not yet been any application of the modeling of RBCs using a technique based on spherical harmonics. However, spherical harmonics has been employed in the development of important science fields. In order to present these applications a multidisciplinary research was performed using the scientific citation indexing service "Web of Science".

2.3.1 Spherical harmonics research in "Web of Science"

Employing the multiple database of "Web of Science" a multidisciplinary search was performed. The areas studied were: Civil Engineering, Engineering Biomedical, Mechanical Engineering, Applied Mathematics and Mechanics.

Applications of Spherical harmonics in Civil Engineering

The published articles related to spherical harmonics applied to Civil Engineering were consulted using the website "Web of Science". Considering as a search filter the parameters presented in Table 2.1. Then a "txt" format file was downloaded with the keywords extracted from the selected articles. Based on this file and with the help of the VOSviewer software the Figure 2.1 was created.

Keywords are located on a circle (Figure 2.1), which will be larger or smaller depending on how many times it is repeated in the selected articles. In addition, using lines and groups of colors (cluster) the keywords that are listed in the articles are linked. Therefore,

Table 2.1: Search criteria for spherical harmonics in Civil Engineering.

Keywords	*spherical harmonics*
Publication years	2011 – 2019
Cathegories	*Engineering civil*
Document type	*Paper*
Total papers	7

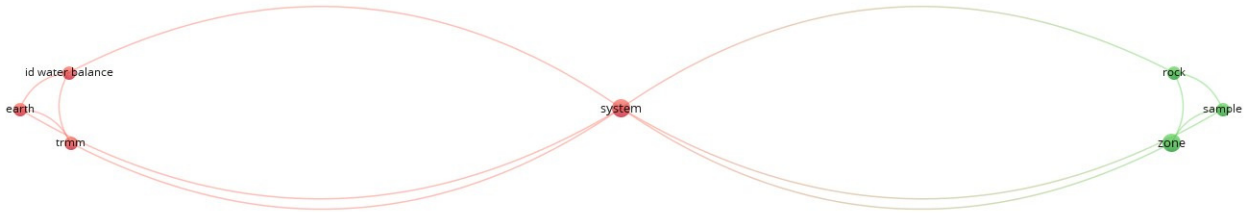

Figure 2.1: Keywords for spherical harmonics in Civil Engineering. Original image from VOSviewer

some observations may be made, allowing the reader to make other annotations according to their topic of interest. The keywords found in the area of Civil Engineering in this case are water balance, earth, system, rock, sample and zone, specifically related to geology, geotechnics, hydrology and structures. Currently authors such as Garboczi, Ahn, Bhanja, Cong, among others are pioneers in the use of SH in civil engineering (Figure 2.2).

In the geotechnical area, for example, Kutay *et al.* (2017) presented a micromechanical model to develop digital microstructures of asphalt mastics and crumb rubber-modified binders, using the dissipative particle dynamics (DPD) model and Xray tomography images of particles to create microstructure. Once the 3D images were generated for individual particle shapes, a series of spherical harmonic (SH) functions were fitted to the surface of the particles and SH coefficients were determined, which allowed effective numerical simulations of DPD to generate microstructures. Moreover, in hydrogeology Liu *et al.* (2012) used the spherical harmonics to express the speed potential in the study of wave diffraction and radiation of a submerged sphere in deep water.

As it can be observed, the use of SH applied to Civil Engineering is small however, its recent use in such diverse and complex subjects reflects its high potential for future research so it is expected that in the coming years the number of publications will increase as shown in Figure 2.3.

Guzas and Earls (2011) for example, implemented the formulation of a beam-column element within a code of explicit non-linear dynamic finite elements to simulate explosive

Figure 2.2: Result Analysis for authors for spherical harmonics in Civil Engineering. Original image from web of science

effects in steel skeletal structures composed of wide-flange members. Using the spherical harmonics, they defined a bounding surface in a stress-resultant space, adjusting the numerical failure data to a basis of a real-valued of SH.

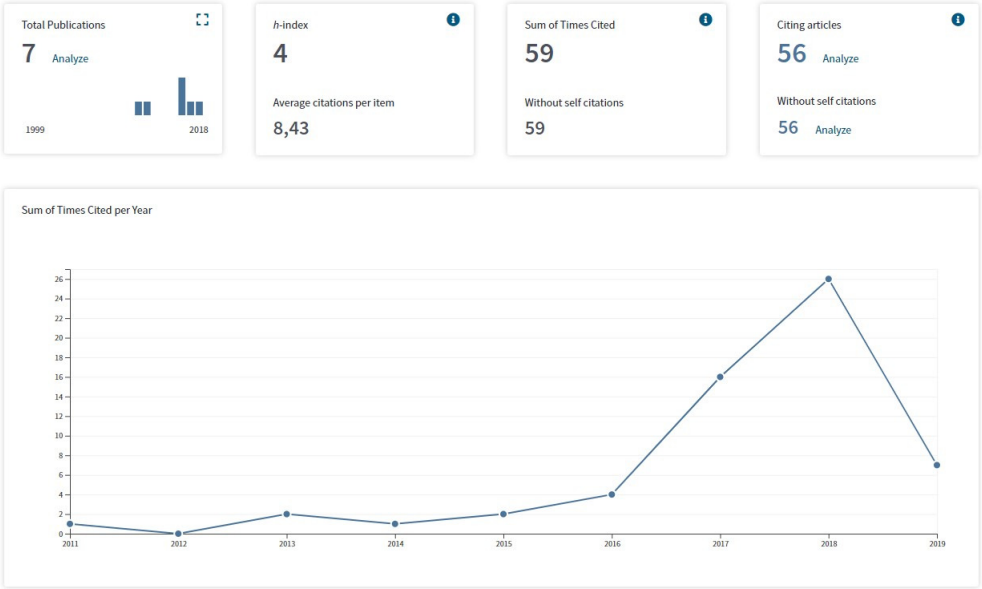

Figure 2.3: Citation report for spherical harmonics in Civil Engineering. Original image from web of science

Applications of Spherical harmonics in Engineering Biomedical

Performing the same procedure explained above and using this time the criteria of Table 2.2, some works were found in the category of biomedical engineering. The keywords found in this review include inverse problem, cell, harmonic, optical tomography

and simulation, gathered in the areas of medicine, biology and engineering (Figure 2.4).

Table 2.2: Search criteria for spherical harmonics in Engineering Biomedical

Keywords	*spherical harmonics*
Publication years	1991 – 2019
Cathegories	*Engineering Biomedical*
Document type	*Paper*
Total papers	67

Figure 2.4: Keywords for spherical harmonics in Engineering Biomedical. Original image from VOSviewer

Figure 2.5 presents the main authors in this field and their publications. For example, Tutar *et al.* (2006) proposed a new method to identify three-dimensional (3-D) prostate boundaries in postimplant ultrasound images in a fast and robust fashion. In this method the segmentation is defined in an optimization framework as fitting the best surface to the underlying images under shape constraints. To derive these constraints, a model of the shape of the prostate was performed using spherical harmonics of degree eight with a statistical analysis on the shape parameters. Xu and Patterson (2006) applied the modified spherical harmonics method to some problems in biomedical optics because is a fast and rigorous solution for the radiative transport equation in an infinite medium containing an isotropic source.

Ayari *et al.* (2014) presented a method to analyze the regional deformation of the heart left ventricle (LV). It consists of two steps. First, a global analysis is carried out in order to detect any pathological cases using 3D spherical harmonic (SPHARM) shape description process. The computed invariant SPHARM shape descriptors are used to compute the distance between the LV anatomical structures namely the endocardium and epicardium. Secondly, to accurately determine the site and the extent of the disease, a regional analysis is achieved. This method has been validated on deformable surfaces synthesized using an ellipsoidal model and real data obtained from myocardial scintigraphy imaging techniques.

Figure 2.5: Result Analysis for authors for spherical harmonics in Engineering Biomedical. Original image from web of science

Chen *et al.* (2015) proposed a hybrid simplified spherical harmonics with diffusion equation (HSDE) based on a diffuse light transport model, in order to reduce the limitations of the simplified spherical harmonics approximation (SPN) and diffusion equation (DE) in describing the light propagation in tissues. The accuracy and efficiency of the HSDE are validated with both regular geometries and digital mouse model-based simulations. Corresponding results reveal that a comparable accuracy and much less computation time are achieved compared with the SPN model as well as a much better accuracy compared with the DE one.

Eck *et al.* (2016) developed a spherical harmonics intensity model for 3D segmentation and 3D shape analysis of heterochromatin foci. The model analytically describes the shape and intensities of the foci, and the parameters are determined by fitting the model to the image intensities using least-squares minimization. Chu *et al.* (2009) developed a light transport model based upon the three-dimensional frequency-domain simplified spherical harmonics (SPN) approximation to improve the accuracy of the commonly used diffusion approximation as used in diffuse optical tomography, because there limits in cases involving strong absorption.

In medicine, Abdolali *et al.* (2017) presents a novel framework for maxillofacial cysts detection. A hybrid methodology based on surface and texture information is introduced. Contourlet and spherical harmonics (SPHARM) coefficients are utilized as texture and shape features which are fed into the classifier. Generally, SPHARM coefficients are estimated by the iterative residual fitting (IRF) algorithm which is based on stepwise regression method. They demonstrated that the proposed methodology can improve the

computer assisted diagnosis (CAD) performance by incorporating more discriminative features. Using orthogonalized SPHARM is promising in computerized cyst detection and may have a significant impact in future CAD systems.

Yang *et al.* (2018) theoretically developed a filtered maximum likelihood expectation maximization (fMLEM) method for bioluminescence tomography (BLT). The method can avoid predefining the permissible source region (PSR) and provide a robust and accurate result for global reconstruction. In the method, the simplified spherical harmonics approximation (SPN) was applied to characterize diffuse light propagation in medium, and the statistical estimation-based MLEM algorithm combined with a filter function was used to solve the inverse problem.

With a significant number of researches using SHs in biomedical engineering, it is possible to observe that each year the number of articles published increases and that their applications tend to expand as the studies advance (Figure 2.6).

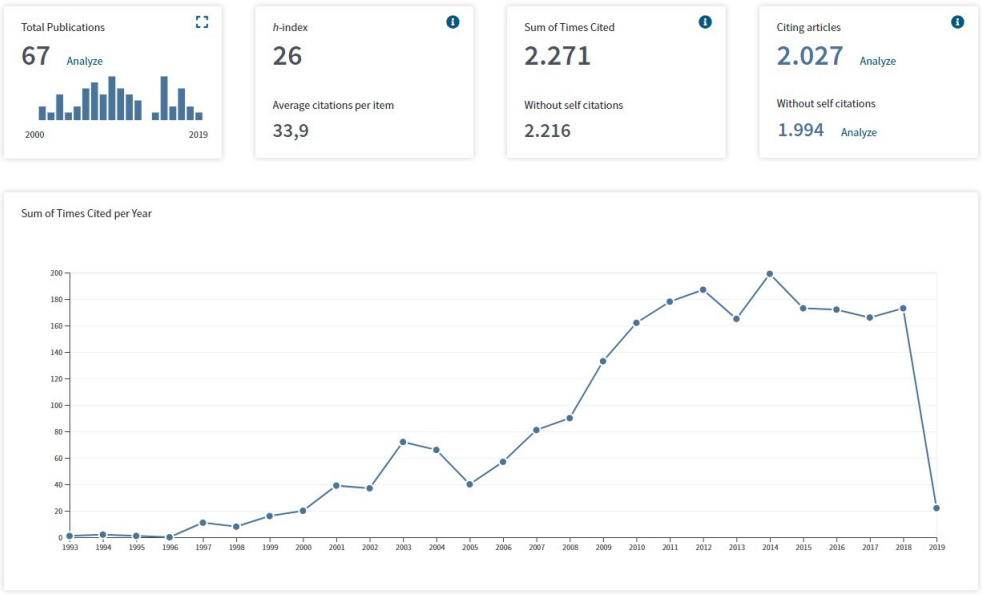

Figure 2.6: Citation report for spherical harmonics in Engineering Biomedical. Original image from web of science

Applications of Spherical harmonics in Applied Mathematics

The spherical harmonics Expansion (SHE) model is a common topic in the Applied Mathematics academic field. Table 2.3 shows the criteria search employed in "Web of Science" service.

Table 2.3: Search criteria for spherical harmonics in Applied Mathematics

Keywords	*spherical harmonics*
Publication years	1962 – 2019
Cathegories	*Applied Mathematics*
Document type	*Paper*
Total papers	367

Figure 2.7 shows the keywords related to spherical harmonics in Applied Mathematics. The publications include: Fourier analysis, inverse problem, between others.

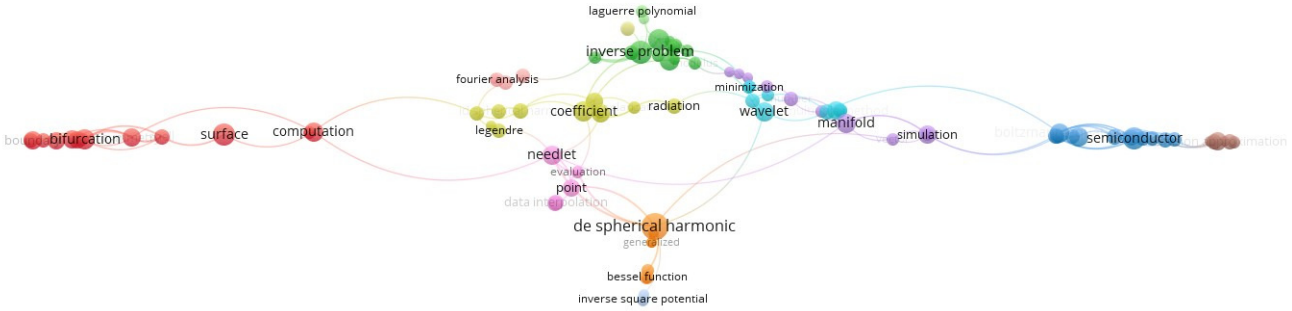

Figure 2.7: Keywords for spherical harmonics in Applied Mathematics. Original image from VOSviewer

Some publications summarizes the state of the art in this area. Figure 2.8 shows the main authors in this field. Potts *et al.* (1998) were one of the firsts ones that mentioned the SHE model as an algorithm for the stable computation of Fourier expansions of square integrable functions on a unit sphere. Whereas, Degond and Schmeiser (1999) established kinetic boundary layers for the SH model boundary conditions semiconductors medium through the semiconductor Boltzmann equation with elastic collisions, and applied the SHE model into a diffusion equation for electron transport in a superlattice (Degond and Zhang, 2002). Abdallah *et al.* (2001) presented an asymptotic analysis of the SHE model for semiconductors considering the mobility and the diffusivity fields.

Kener and Potts (2008) established a new process in order to improve the fast algorithm for the evaluation of spherical harmonic expansions through quadrature rules. Potts *et al.* (2009) introduced a fast algorithm for Fourier transform applied into the nonequispaced nodes on the three-dimensional torus. Graf and Potts (2009) developed a complementary procedure to improve the fast algorithm for Fourier transform on the rotation group. Menegatto and Piantella (2011) provided an overview on the Laplace-Beltrami derivate used in the SHE models. Haskovec *et al.* (2011) proved that SHE model

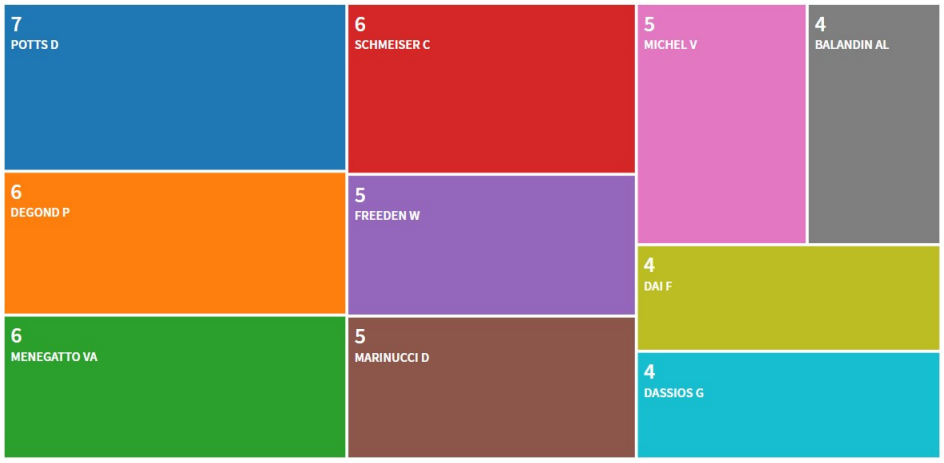

Figure 2.8: Result Analysis for authors for spherical harmonics in Applied Mathematics. Original image from web of science

can be coupled with the poisson equation for a strong convergence to equilibrium in the analysis.

More recently, Jordão and Menegatto (2014) studied the action of the weighted Fourier-Laplace transform on the functions in the kernel Hilbert space (RKHS) taking into account the smoothness of the SHE model generated elements. Cammarota *et al.* (2016) presented a second-order Gaussian kinematic formula for the excursion set of random spherical harmonics through the asymptotic variance of the Euler-Poincare characteristic. Dai *et al.* (2016) determined the sharp asymptotic order of some Holder inequality for Spherical Harmonics in order to improve the inequalities for the Fourier transform. Campese *et al.* (2018) worked with high-energy hyperspherical eigenfunctions applied to the She model through non-Gaussian models. Leweke *et al.* (2018) applied the SHE model to find Slepian functions that are at least optimally spatio-spectrally localized on a representation of a real-valued vector fields on a three dimensional ball.

Figure 2.9 shows the citation report for Applied Mathematics. It is possible to identify a great number of publications, around 367 as well as the increase in citations per year.

Applications of Spherical harmonics in Mechanical Engineering

Approaching the Mechanical Engineering field, the search was performed using the information shown in Table 2.4.

Regarding the Mechanic Engineering field, a number of studies have explored the usage of the spherical harmonic analysis as an alternative approach to solve different types of

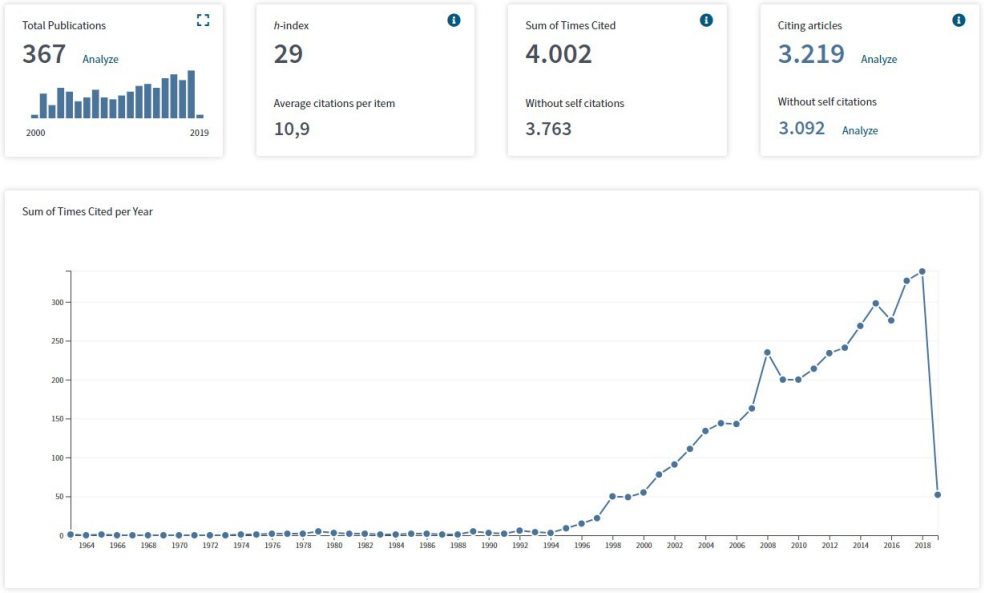

Figure 2.9: Citation report for spherical harmonics in Applied Mathematics. Original image from web of science

Table 2.4: Search criteria for spherical harmonics in Mechanical Engineering

Keywords	*spherical harmonics*
Publication years	1989 – 2019
Cathegories	*Mechanical Engineering*
Document type	*Paper*
Total papers	62

problems, more specifically, modeling different phenomena at a relative low computational effort without a significant impact on the accuracy (Allu and Mazumder, 2018; Ge *et al.*, 2015; Pal and Modest, 2015). As shown in Figure 2.10, spherical harmonics has been applied in studies of noise, displacement function, heat transfer applications, between others.

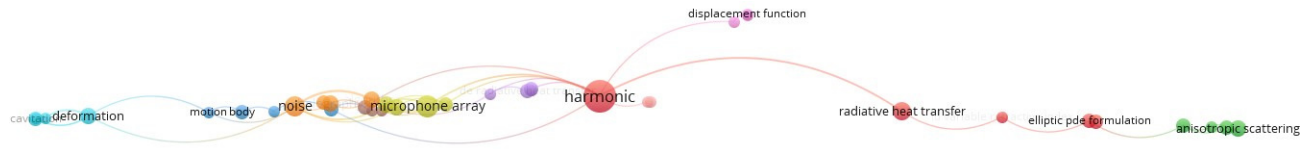

Figure 2.10: Keywords for spherical harmonics in Mechanical Engineering. Original image from VOSviewer

According to Figure 2.11, Modest, MF (Modest *et al.*, 2014) and Mazumder S (Sankar and Mazumder, 2012) appear as the main authors in this area. Modest and Cai Modest *et al.* (2014) used a Simplified Spherical Harmonics method (SP_n) for radiative heat transfer applications. This resulted in the reduction of the ruling set of equations to a

small set of second-order, elliptic PDEs, almost similar to a simple legendre polynomial (P_1 approximation). The method presents considerable savings in terms of computational effort when compared to a P_n model. Allu and Mazumder (2016) modeled the transport of heat in semiconductor materials using the lowest order spherical harmonics method (P_1 approximation).

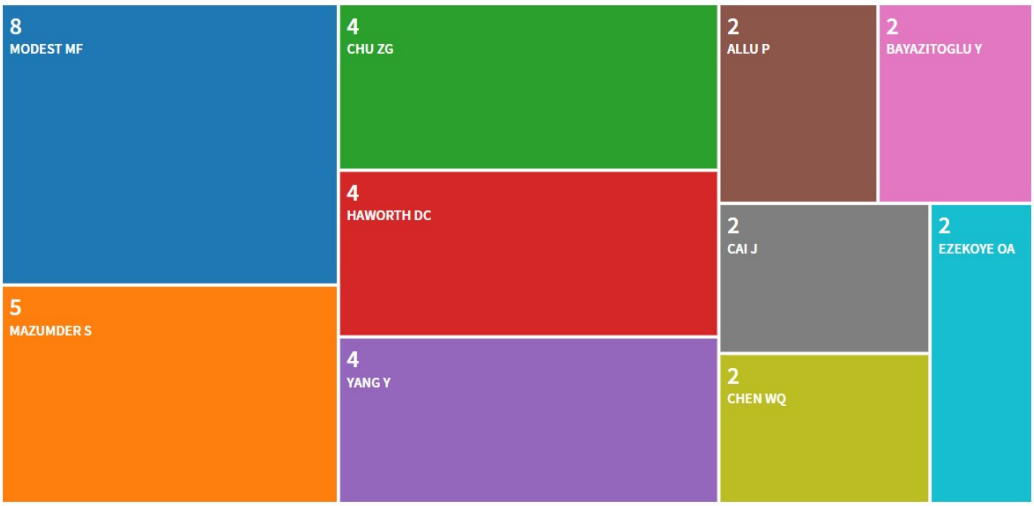

Figure 2.11: Result Analysis for authors for spherical harmonics in Mechanical Engineering

Overall, it is clear that a spherical harmonics approach represents an appealing alternative to model phenomena in which the computational effort and accuracy are key factors. The adaptability of this type of approach is certainly an important feature that makes it useful in different research areas.

Finally, Figure 2.12 is shown as a report of all articles published in this field. 62 publications were analyzed. It is possible to assume the increase interest in the spherical harmonics study in recent years.

Applications of Spherical harmonics in Mechanics

In the field of Mechanics, spherical harmonics are also a very important tool for modeling purposes. As in most of the previous cases, its ease of implementation and the reasonable computational efficiency are considered important features. The search criteria are presented in Table 2.5.

Some Keywords in this field related to spherical harmonics are shown in Figure 2.13.

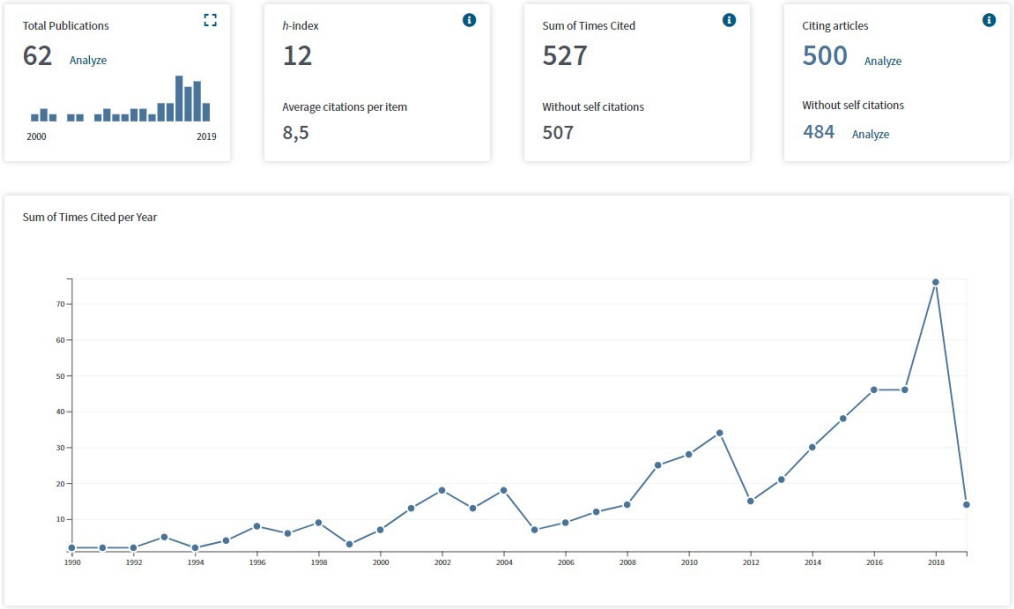

Figure 2.12: Citation report for spherical harmonics in Mechanical Engineering . Original image from web of science

Table 2.5: Search criteria for spherical harmonics in Mathematics applied

Keywords	*spherical harmonics*
Publication years	1962 – 2019
Cathegories	*Mechanics*
Document type	*Paper*
Total papers	160

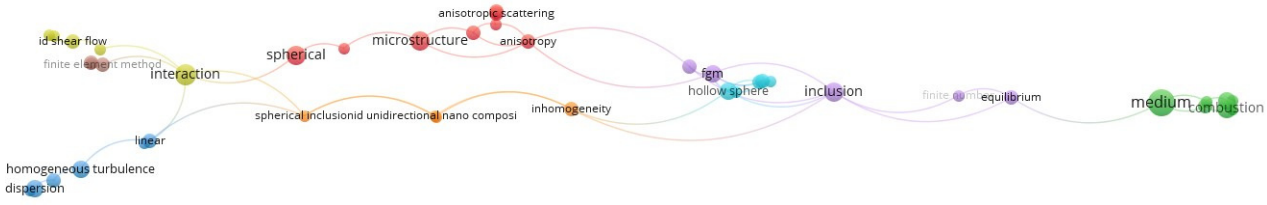

Figure 2.13: Keywords for spherical harmonics in Mechanics. Original image from VOSviewer

In Chen (2000), the author expands three displacement functions in terms of spherical harmonics in order to simplify its basics equations. This procedure is performed in order to model a steadily rotating spherical shell. Furthermore, Cambon et al. Mons *et al.* (2016) models the homogenous shear-driven anisotropic turbulence using spherical harmonics to expand the spectral two-point velocity correlation. A detailed analysis of Cambon's work is presented in Briard *et al.* (2018). Crouch and Kushch Kushch *et al.* (2013) studied elastics fields and presented a representative unit cell model (RUC) of

nanocomposite. Using local expansions of the displacement and stressed fields in terms of spherical harmonics, they managed to reduce the problem to an infinity system of linear equations, which are then truncated and solved numerically.

The main authors in Mechanics applications are presented in Figure 2.14. Risso, Chebel, and Masbernat Lalanne *et al.* (2015) analyzed the shape-oscillations of a gas bubble or a liquid drop rising in a different liquid. The bubble (drop) is attached to a capillary and eventually released, which results in the rising of the bubble (drop) plus the oscillation of its shape. A decomposition of the shape of the bubble (drop) into a series of spherical harmonics permits to compare experimental observations and numerical simulations. As an extended work, a similar approach is used to study the effect of the rising motion on the dynamics of shape oscillations of drops and bubbles Lalanne *et al.* (2013).

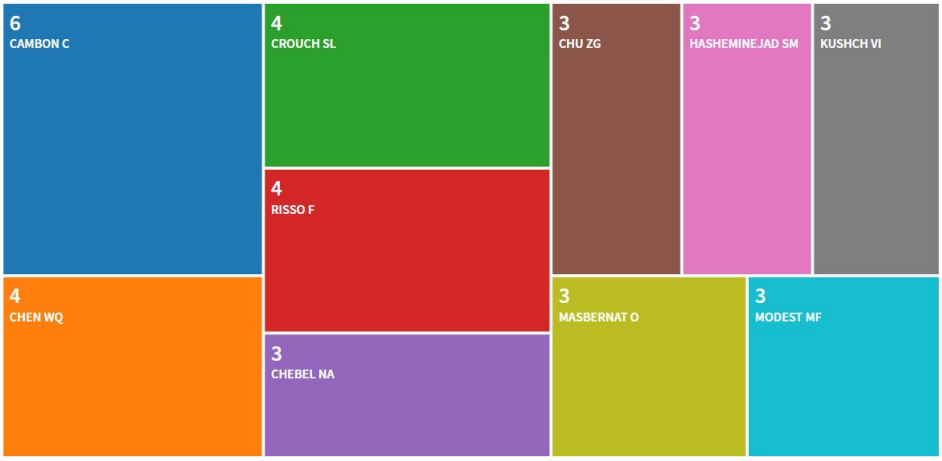

Figure 2.14: Result Analysis for authors for spherical harmonics in Mechanics. Original image from web of science

Based on these few examples, it is possible to notice the importance of spherical harmonics at different stages of the modelling process. It is also clear that further studies are required in order to determine new areas of application.

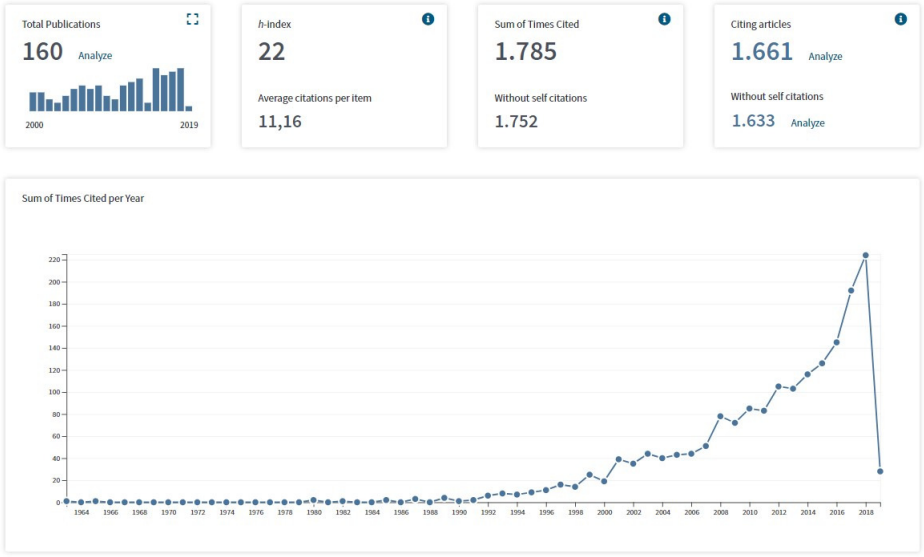

Figure 2.15: Citation report for spherical harmonics in Mechanics. Original image from web of science

Chapter 3

Shell Theory

In a continuum model, an RBC is treated as a thin shell. A shell element is described by an inner surface and two outer surfaces such that a normal to the inner (middle) surface intersects with both outer surfaces at the same distance as shown in Figure 3.1. Shells can be modeled appropriately by means of classical Kirchhoff kinematics, based on the following assumptions:

- The shell formulation is derived as a two-dimensional surface instead of a three-dimensional continuum.
- The director describes the thickness extension.
- Points that lie on one and the same normal to the undeformed middle surface also lie on one and the same normal to the deformed middle surface.
- The displacements in the direction of the normal to the middle surface are equal for all points on the same normal.

In this work, matrix and tensor notation are used. Italic letters a and A indicate scalars, lower case bold letters $\mathbf{a}$ indicate vectors, and upper case bold letters $\mathbf{A}$ indicate second-order tensors.

3.1 Basic notions of tensor calculus

Tensor calculus will be used widely throughout this work. This section introduces some important aspects that will be used in the formulations presented in this chapter. The use of tensors may be justified by the main properties of tensors equations. As stated in Niordson (1985), a tensor equation does not refer to any particular coordinate system; if the equation holds in one system, it holds in all.

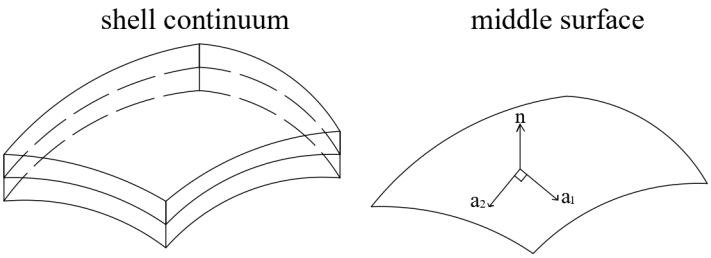

Figure 3.1: Representation of the middle surface

Any formulation expressed in Cartesian coordinates using tensor analysis holds for surface coordinates, and the reverse also applies. Thus, one can preserve the geometric perspective while taking advantage of different coordinate systems. Also, tensor notation often helps to systematize calculations due to its compactness, and despite this characteristic, tensor notation also offers robust and explicit expressions.

To achieve invariance, coordinate transformations must be defined to form expressions that result in the same value in all coordinate systems. Latin letters are used to describe variables in the ambient three-dimensional space, e.g., components of a vector position x^i $(i = 1, 2, 3)$, whereas Greek letters are used for two-dimensional surface embedded in the ambient space, e.g., u^α $(\alpha = 1, 2)$.

Using the definition in Grinfeld (2010), the position vector $\mathbf{r}$ is a function of coordinates x^i that uniquely determine a point in space.

$$\mathbf{r} = \mathbf{r}\left(x^i\right) \tag{3.1}$$

The covariant basis $\mathbf{z_i}$ is obtained from the position vector by differentiation with respect to each of the coordinates:

$$\mathbf{z_i} = \frac{\partial \mathbf{r}}{\partial x^i} \tag{3.2}$$

Then, any other vector $\mathbf{v}$ can be expressed as

$$\mathbf{v} = v^i \mathbf{z}_i \tag{3.3}$$

The values v^i are called the contravariant components of the vector. The components of the covariant metric tensor Z_{ij} are defined as

$$Z_{ij} = \mathbf{z_i} \cdot \mathbf{z_j} \tag{3.4}$$

It is often referred to as the fundamental tensor because information can be retrieved from it regarding the fundamental properties of the space. The contravariant metric tensor Z^{ij} is the matrix inverse of Z^{ij}, and the contravariant basis $\mathbf{z}^i$ is defined as follows:

$$\mathbf{z}^i = Z^{ij}\mathbf{z}_j \tag{3.5}$$

The covariant and contravariant bases are related by the following condition:

$$\mathbf{z}_i \cdot \mathbf{z}^j = \delta^i_j = \begin{cases} 0 & i \neq j \\ 1 & i = j \end{cases} \tag{3.6}$$

A tensor $\mathbf{M}$ can be expressed using two different covariant bases, $\mathbf{s}_\alpha \otimes \mathbf{s}_\beta$ and $\mathbf{z}_i \otimes \mathbf{z}_j$, as follows:

$$\mathbf{M} = M^{\alpha\beta}\mathbf{s}_\alpha \otimes \mathbf{s}_\beta = M^{ij}\mathbf{z}_i \otimes \mathbf{z}_j \tag{3.7}$$

where $\otimes$ is the tensorial (dyadic) product. Likewise, for contravariant bases,

$$M = M_{\alpha\beta}\mathbf{s}^\alpha \otimes \mathbf{s}^\beta = M_{ij}\mathbf{z}^i \otimes \mathbf{z}^j \tag{3.8}$$

Using the shift tensor, the components in the ambient surface are obtained by

$$M^{ij} = z^i_\alpha z^j_\beta M^{\alpha\beta} \tag{3.9}$$

and

$$M_{ij} = z^\alpha_i z^\beta_j m_{\alpha\beta} \tag{3.10}$$

The last two equations provide the transformation rules needed in the following sections. As stated in Niordson (1985), one must not restrict oneself to Cartesian coordinates only, especially in shell theory, in which two-dimensional coordinate systems should be used since the shape of a shell is described by the middle surface and the shell thickness h.

3.2 The geometry of the middle surface

The middle surface is a surface such that any normal to it intersects the two free surfaces of the shell. A two-dimensional surface embedded in a three-dimensional space is defined by the tangent and normal spaces that exist at all points on the surface. The tangent space is two-dimensional, and the normal space is one-dimensional and is represented by the unit normal vector $\mathbf{n}$.

The surface is described parametrically by $a^\alpha = (\theta, \phi)$ (3.1) and the Cartesian coordinates $x^i = (x, y, z)$, which depend on a^α by three independent, single-valued, continuously differentiable functions. Consider the position vector $\mathbf{r}$ as a function of surface coordinates:

$$\mathbf{r}(x^i(a^\alpha)) \tag{3.11}$$

In this case, the covariant basis $\mathbf{a}_\alpha$ is expressed as

$$\mathbf{a}_\alpha = \frac{\partial \mathbf{r}}{\partial a^\alpha} \tag{3.12}$$

Applying the chain rule, one obtains

$$\mathbf{a}_\alpha = \frac{\partial \mathbf{r}}{\partial x^i}\frac{\partial x^i}{\partial a^\alpha} = Z^i_\alpha \mathbf{Z}_i \tag{3.13}$$

$Z^i_\alpha = \partial x^i / \partial a^\alpha$ relates the surface and Cartesian bases and represents the tangent space. It is known as the shift tensor because it translate or 'shifts' components of the tangent vector from the surface coordinates into Cartesian space. That is, for any $\mathbf{t}$ tangent to the surface,

$$t^i = t^\alpha Z^i_\alpha, \; t^\alpha = t^i Z^\alpha_i \tag{3.14}$$

The expression for obtaining the surface covariant metric coefficients of the fundamental tensor is

$$a_{\alpha\beta} = \mathbf{a}_\alpha \cdot \mathbf{a}_\beta \tag{3.15}$$

The lengths of arcs and angles between curves can be expressed in terms of $a_{\alpha\beta}$. The Cartesian basis and the surface covariant fundamental tensor are related as follows:

$$a_{\alpha\beta} = Z_{ij} Z^i_\alpha Z^j_\beta \tag{3.16}$$

The contravariant basis vectors are

$$\mathbf{a}^\alpha = a^{\alpha\beta}\mathbf{a}_\beta \tag{3.17}$$

with

$$\left[a^{\alpha\beta}\right] = \left[a_{\alpha\beta}\right]^{-1} \tag{3.18}$$

The normal direction is captured by the normal $\mathbf{n}$, with components n^i. A normal to the surface is perpendicular to the tangent plane and hence to both vectors $\mathbf{a}_1$ and $\mathbf{a}_2$. A unit normal vector of the middle surface is expressed as follows:

$$\mathbf{n} = \frac{\mathbf{a}_1 \times \mathbf{a}_2}{|\mathbf{a}_1 \times \mathbf{a}_2|} \tag{3.19}$$

Another important property that describes the middle surface is the second fundamental or curvature tensor of the surface, $b_{\alpha\beta}$, which is symmetrical, as is the first fundamental tensor. The curvature tensor serves to define extrinsic invariants of the surface. The coefficients are obtained from the definition of the covariant derivative of the covariant basis, as follows:

$$b_{\alpha\beta} = -Z^i_\alpha \nabla_\beta n^i \tag{3.20}$$

where $\nabla_\alpha(\cdot)$ is the covariant derivative of $(\cdot)$.

3.3 Shell continuum

A point in the shell continuum can be uniquely identified by the coordinates a^α and the distance z from the middle surface as measured along a normal to that point. In Cartesian coordinates, the point is given by

$$\mathbf{x} = \mathbf{r}(a^1, a^2) + z\mathbf{n} = f^i(a^1, a^2, a^3) \tag{3.21}$$

In particular, $z = \pm\frac{1}{2}h$ represents the free surfaces of the shell. The covariant basis at a point in the shell continuum is defined by

$$\mathbf{g}_\alpha = \frac{\partial \mathbf{r}}{\partial a^\alpha} + z\frac{\partial \mathbf{n}}{\partial a^\alpha} = \mathbf{a}_\alpha + z\nabla_\alpha \mathbf{n} \tag{3.22}$$

$$\mathbf{g}_3 = \mathbf{n} \tag{3.23}$$

The components of the three-dimensional covariant metric tensor in the shell continuum are given by the dot product of the covariant bases:

$$g_{ij} = \mathbf{g}_i \cdot \mathbf{g}_j = \frac{\partial f^k}{\partial a^i} \cdot \frac{\partial f^k}{\partial a^j} \tag{3.24}$$

Since $\mathbf{n}$ and $\mathbf{a}_\alpha$ are orthogonal, one can use expression (3.18) for the curvature tensor to obtain

$$g_{33} = g^{33} = 1, \; g_{\alpha 3} = g^{\alpha 3} = 0 \tag{3.25}$$

$$g_{\alpha\beta} = \frac{\partial f^k}{\partial a^\alpha} \cdot \frac{\partial f^k}{\partial a^\beta} = a_{\alpha\beta} - 2b_{\alpha\beta}z + b^\gamma_\alpha b_{\gamma\beta}(z)^2 \tag{3.26}$$

For a thin shell, the quadratic term can be neglected under the assumption of a linear distribution throughout the thickness. Then,

$$g_{\alpha\beta} = a_{\alpha\beta} - 2b_{\alpha\beta}z \tag{3.27}$$

Finally, the contravariant metric tensor at a point in the shell continuum is obtained as follows:

$$g^{\alpha\beta} = [g_{\alpha\beta}]^{-1} \tag{3.28}$$

3.4 Kinematics

Everything stated up to this point holds for both undeformed and deformed configurations. In the following formulation, the Lagrangian description is used to define the modes of deformation. Thus, the deformation is described using the coordinates of a typical point in the initial state.

The Cartesian components of the displacement vector of a point on the middle surface after deformation are

$$v^i = f^i_{,\alpha} v^\alpha + N^i v^3 \tag{3.29}$$

where v^α is a vector field defining the tangential displacements and v^3 is a scalar field defining the normal displacements; here, partial derivatives are denoted by $(\cdot)_{,i} = \partial(\cdot)/\partial x^i$.

Usually, the motion behavior in the neighborhood of a point is expressed as a function of geometric quantities in the deformed and undeformed configurations. Variables denoted by $(\cdot)_o$ refer to the undeformed configuration.

The deformation of a shell is described by the stretching and bending of the middle surface. A measure of the change in the distance between two neighboring points on the middle surface may be expressed in terms of the strain tensor $\epsilon_{\alpha\beta}$, defined by

$$\epsilon_{\alpha\beta} = \frac{1}{2}\left(a_{\alpha\beta} - a_{0\alpha\beta}\right) \tag{3.30}$$

and similarly, the bending tensor $\kappa_{\alpha\beta}$, given by

$$\kappa_{\alpha\beta} = b_{\alpha\beta} - b_{0\alpha\beta} \tag{3.31}$$

can be used to describe changes in curvature.

For a point in the shell continuum, the deformation gradient $\mathbf{F}$, a primary measure of deformation, characterizes the motion behavior in the neighborhood of that point, including rigid-body motions. The deformation gradient is defined as

$$\mathbf{F} = \frac{d\mathbf{x}}{d\mathbf{x}_0} \tag{3.32}$$

For curvilinear coordinates,

$$\mathbf{F} = \mathbf{g}_i \otimes \mathbf{g}_0^i \tag{3.33}$$

$$\mathbf{F}^{-1} = \mathbf{g}_{0i} \otimes \mathbf{g}^i \tag{3.34}$$

Another measure of strain is the right Cauchy-Green tensor $\mathbf{C}$:

$$\mathbf{C} = \mathbf{F}^T\mathbf{F} = C_{ij}\mathbf{g}_0^i \otimes \mathbf{g}_0^j \tag{3.35}$$

This tensor is a measure of the strain in the material coordinates, where

$$C_{ij} = \begin{pmatrix} a_{11} & a_{12} & 0 \\ a_{21} & a_{22} & 0 \\ 0 & 0 & C_{33} \end{pmatrix} \tag{3.36}$$

For an incompressible hyperelastic material, the following expression for C_{33} is found in Kiendl *et al.* (2015):

$$C_{33} = J_0^{-2} \tag{3.37}$$

where J_0 is defined as the in-plane determinant, expressed as

$$J_0 = \sqrt{\frac{|a_{\alpha\beta}|}{|a_{0\alpha\beta}|}} \tag{3.38}$$

$\mathbf{C}$ can be used to obtain an expression for the Green-Lagrange strain tensor $\mathbf{E}$ as follows:

$$\mathbf{E} = \frac{1}{2}(\mathbf{C} - \mathbf{I}) \tag{3.39}$$

$\mathbf{E}$ enables the evaluation of changes in length relative to the undeformed state; thus, $\mathbf{I}$ is the identity tensor in the undeformed state. Accordingly, the components E_{ij} of the

strain tensor are defined by

$$E_{ij} = \frac{1}{2}\left(C_{ij} - g_{0ij}\right) \tag{3.40}$$

Thus,

$$\mathbf{E} = E_{ij}\mathbf{g}_0^i \otimes \mathbf{g}_0^j \tag{3.41}$$

Only the in-plane strain components, $E_{\alpha\beta}$, are considered for shell kinematics:

$$E_{\alpha\beta} = \frac{1}{2}\left((a_{\alpha\beta} - a_{0\alpha\beta}) - 2z(b_{\alpha\beta} - b_{0\alpha\beta})\right) \tag{3.42}$$

Finally, the strain in the shell continuum is expressed as

$$E_{\alpha\beta} = \epsilon_{\alpha\beta} + z\kappa_{\alpha\beta} \tag{3.43}$$

Chapter 4

Constitutive Relations

The relationships between strains and stresses are described by constitutive equations. The kinematics and formulations presented in the previous chapter are valid for a shell element of any type of material. In this section, constitutive equations for hyperelastic and viscoelastic materials are presented that are applicable for large-strain analyses. Constitutive models of this kind are commonly used for the simulation of biological membranes such as RBCs.

For the hyperelastic model, the second Piola-Kirchhoff stress tensor $\mathbf{S}$ is used to derive the constitutive equations. For the viscoelastic constitutive equations, the Kelvin-Voigt model is used, and an explicit method of implementation is described.

In Skalak *et al.* (1973), it was shown that an RBC membrane cannot change thickness in response to an in-plane stress, but rather, only the shape of a surface element can change; that is, it is isotropic in the plane of the membrane. Because of the fixed thickness, applied forces are considered to be distributed in a per-unit-length manner. Therefore, the constitutive relations will be expressed in the form of resultant quantities vs. deformation (Evans and Hochmuth, 1976).

4.1 Hyperelastic model

The material of an RBC is able to recover to its original undeformed state after undergoing high-order deformations; thus, it falls within the definition of a hyperelastic material. For an isotropic hyperelastic material, the existence of a strain-energy function Ψ is postulated, which describes the strain energy per unit volume under deformation.

Ψ is a scalar-valued function of one tensor variable, such as $\mathbf{F}$, $\mathbf{C}$ or $\mathbf{E}$, and is assumed to be continuous. To express the internal energy of a body, any stress measure can be used. However, this variable cannot be selected arbitrarily. Each stress tensor is related to a defined strain tensor through the rate of change in the internal energy. The second Piola-Kirchhoff stress tensor $\mathbf{S}$ is expressed as

$$\mathbf{S} = S^{ij}\mathbf{g}_0^i \otimes \mathbf{g}_0^j \tag{4.1}$$

and is energetically conjugate to the Green-Lagrange strain tensor. Therefore, it is used to define the constitutive equation for a hyperelastic material, in the so-called 'Green elastic material model'. The constitutive equation considered to describe this model is (Holzapfel, 2000)

$$S^{ij} = \frac{\partial \Psi}{\partial E_{ij}} = 2\frac{\partial \Psi}{\partial C_{ij}} \tag{4.2}$$

The relation

$$\boldsymbol{\sigma} = J^{-1}\mathbf{F}\mathbf{S}\mathbf{F}^T \tag{4.3}$$

is the explicit expression for calculating the symmetric Cauchy or true stress tensor $\boldsymbol{\sigma}$, where J is the determinant of the deformation gradient and can be computed as follows:

$$J = \det\mathbf{F} = \sqrt{\det\mathbf{C}} \tag{4.4}$$

The second Piola-Kirchhoff stress tensor relates the forces to the deformed area, whereas the Cauchy stress tensor relates them to the original configuration. The invariants of $\mathbf{C}$ are needed for some hyperelastic models. In terms of the components of $\mathbf{C}$, the invariants are expressed as follows:

$$\begin{gathered} I_1 = \mathrm{tr}(\mathbf{C}) = C_{11} + C_{22} + C_{33} \\ I_2 = C_{11}C_{22} + C_{22}C_{33} + C_{33}C_{11} - C_{12}C_{21} - C_{23}C_{32} - C_{13}C_{31} \\ I_3 = \det\mathbf{C} = C_{11}C_{22}C_{33} + 2C_{12}C_{23}C_{13} - C_{11}C_{23}C_{32} - C_{22}C_{13}C_{31} - C_{33}C_{12}C_{21} \end{gathered} \tag{4.5}$$

Ψ is assumed to have continuous derivatives with respect to the principal invariants I_i of the tensor $\mathbf{C}$. Using the chain rule, it is possible to find that

$$\frac{\partial I_1}{\partial \mathbf{C}} = \mathbf{I} \tag{4.6}$$

$$\frac{\partial I_2}{\partial \mathbf{C}} = I_1\mathbf{I} - \mathbf{C} \tag{4.7}$$

$$\frac{\partial I_3}{\partial \mathbf{C}} = I_3\mathbf{C}^{-1} \tag{4.8}$$

Thus, the most general form of a stress relation in terms of the invariants of $\mathbf{C}$ for an isotropic hyperelastic material at finite strain is

$$\mathbf{S} = 2\frac{\partial \Psi}{\partial \mathbf{C}} = 2\left[\left(\frac{\partial \Psi}{\partial I_1} + I_1\frac{\partial \Psi}{\partial I_2}\right)\mathbf{I} - \frac{\partial \Psi}{\partial I_2}\mathbf{C} + I_3\frac{\partial \Psi}{\partial I_3}\mathbf{C}^{-1}\right] \tag{4.9}$$

An RBC is a very thin bilayer lined with a protein network. It behaves as a two-dimensional incompressible elastic sheet with nonlinear constitutive behavior.

For the study of materials that maintain a constant volume throughout their motion, the incompressibility constraint, $J = 1$, must be considered. Therefore, the strain-energy function is defined as follows:

$$\Psi = \Psi(\mathbf{C}) - p(J-1) \tag{4.10}$$

where the scalar p is a Lagrange multiplier, identified as a hydrostatic pressure. Thus, for the constitutive equation, one has

$$S^{ij} = 2\frac{\partial \Psi}{\partial C_{ij}} = 2\left(\frac{\partial \Psi}{\partial C_{ij}} - \frac{\partial p}{\partial C_{ij}}(J-1) - p\frac{\partial J}{\partial C_{ij}}\right) \tag{4.11}$$

According to Equation (4.4) and with the application of the chain rule, the derivative of the Jacobian determinant is obtained as follows:

$$\frac{\partial J}{\partial C_{ij}} = \frac{1}{2}JC^{ij} \tag{4.12}$$

Then, for incompressible hyperelasticity,

$$S^{ij} = 2\frac{\partial \Psi}{\partial C_{ij}} - pC_{ij} \tag{4.13}$$

For the shell model, to satisfy the plane stress conditions, C_{33} needs to be determined such that $S^{33} = 0$. Applying this restriction results in the following expression for p:

$$p = 2\frac{\partial \Psi}{\partial C_{33}}C_{33} \tag{4.14}$$

Then, using Equation (3.35), the in-plane components of the second Piola-Kirchhoff stress tensor are obtained as follows:

$$S^{\alpha\beta} = 2\frac{\partial \Psi}{\partial C_{\alpha\beta}} - 2\frac{\partial \Psi}{\partial C_{33}}(J_0)^{-2}g^{\alpha\beta} \tag{4.15}$$

Finally, the components of the resultant membrane and bending stresses for the hyperelastic incompressible model, in local coordinates, are obtained via integration through the thickness:

$$t^{\alpha\beta} = \int_{-h/2}^{h/2} S^{\alpha\beta} dz \tag{4.16}$$

$$m^{\alpha\beta} = \int_{-h/2}^{h/2} S^{\alpha\beta} z dz \tag{4.17}$$

4.1.1 Strain-energy functions

Several attempts have been made to describe the nonlinear stress–strain behaviors of complex materials such as rubbers, polymers, and biological tissues. A combination of strain invariants can be used to mathematically define the strain-energy function to represent the mechanical behavior of so-called rubber-like materials.

The strain-energy function for the Mooney-Rivlin model (Mooney, 1940) is

$$\Psi = c_1 (I_1 - 3) + c_2 (I_2 - 3) \tag{4.18}$$

where I_1 and I_2 are the invariants of the right Cauchy-Green tensor $\mathbf{C}$. The authors of this model stated that just as two constants, the modulus of rigidity and the Poisson ratio, are required to characterize the infinitesimal deformation of an elastic material, so are two constants, c_1 and c_2, required to characterize the moderate deformation of a *superelastic* material. c_1 and c_2 are empirically determined and are related to the linear elastic shear modulus G.

In Rivlin and Rideal (1948), further developments in the general theory of highly elastic materials were presented, and a model similar to Hooke's law was introduced, called the neo-Hookean model. The strain-energy function takes the following form:

$$\Psi = c_1 (I_1 - 3) \tag{4.19}$$

where c_1 is a material constant. Using (3.9) for the partial derivatives of Ψ and (3.15) for the in-plane components, one obtains the following stress-strain relations for the Mooney-Rivlin model:

$$S^{\alpha\beta} = 2c_1 \left(g_0^{\alpha\beta} - J_0^{-2} g^{\alpha\beta} \right) + 2c_2 J_0^{-2} \left(g_0^{\alpha\beta} - g_{\alpha\beta} g_0^{\alpha\beta} g^{\alpha\beta} \right) \tag{4.20}$$

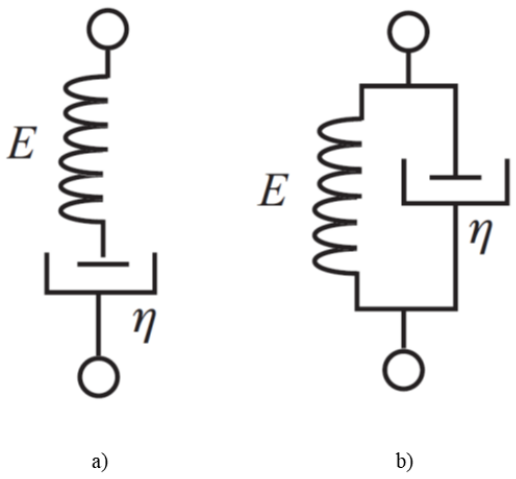

Figure 4.1: Spring-dashpot models. a) Maxwell b)Kelvin-Voigth. Lakes (2009)

Similarly, the following relations are obtained for the neo-Hookean model:

$$S^{\alpha\beta} = 2c_1 \left(g_0^{\alpha\beta} - J_0^{-2} g^{\alpha\beta} \right) \tag{4.21}$$

The equations described above considered a material description. In practice, the Cauchy stresses are of engineering significance. A spatial description can be found in Bonet *et al.* (2016)

4.2 Membrane viscosity

In modeling an RBC, it is important to consider that the membrane has a finite viscosity. Viscoelastic behavior is understood as the capacity to return to the initial geometry when the load is removed; however, this state is reached only after a certain amount of time. Thus, any deformation depends on time.

Viscoelastic materials are those for which the relationship between stress and strain depends on time. The spring-dashpot models are commonly used with an acceptable outcome, represented by a perfectly elastic spring with an elastic modulus E and a perfectly viscous dashpot, with η as viscosity. The Maxwell model consists of a spring and dashpot in series. The total deformation, or strain, is the sum of the strains in both elements. The Kelvin-Voigt model consist of a spring and dashpot in parallel so that they both experience the same deformation or strain. The total stress is also the sum of the stresses in each element. Both models are shown in Figure 4.1 (Lakes, 2009).

When an RBC is suspended in a shear flow, it deforms under the influence of the viscous stresses exerted by the suspending medium. In this work, the Kelvin-Voigt model is assumed. This model consists of a spring and a dashpot in parallel such that both experience the same deformation or strain and the total stress is the sum of the stresses on each element.

According to Yazdani and Bagchi (2013), the membrane response is likely to be more complicated than that of the Kelvin-Voigt model; however, this model has the advantages of being simple and introducing a single constant parameter. The stress tensor is the sum of the elastic and viscous contributions:

$$\boldsymbol{\sigma} = \boldsymbol{\sigma}^e + \boldsymbol{\sigma}^v \tag{4.22}$$

If the shell is incompressible, as is the case for many biological membranes with a bilayer structure, only the pure shear components of the strain rate are relevant. For a two-dimensional membrane with a surface viscosity μ^s, the viscous contribution is (Barthes-Biesel and Sgaier, 1985)

$$\boldsymbol{\sigma}^v = 2\mu^s \mathbf{e} \tag{4.23}$$

where $\mathbf{e}$ is the strain rate tensor and depends on the velocity field $\mathbf{v}$. Then, the Cartesian components of $\mathbf{e}$ are defined as

$$e_{ij} = \frac{1}{2}\left[\frac{\partial v_i}{\partial x_j} + \frac{\partial v_j}{\partial x_i}\right] \tag{4.24}$$

Following Barthes-Biesel and Sgaier (1985), one of the approaches to coupling the fluid and solid mechanics is to ensure the continuity of velocities between the liquid and the membrane, i.e.,

$$\mathbf{v}^f = \mathbf{v}^m \tag{4.25}$$

where

$$\mathbf{v}^m = \frac{d\mathbf{x}}{dt} \tag{4.26}$$

and $\mathbf{v}^f$ represents the fluid velocity on the surface.

Under the assumption of a constant velocity throughout the thickness, the total stress $\boldsymbol{\sigma}$ is also constant; however, the deformation gradient must be calculated at each Gauss point throughout the thickness. Thus,

$$\mathbf{S} = J\mathbf{F}^{-1}\boldsymbol{\sigma}\mathbf{F}^{-T} \tag{4.27}$$

Finally, the resultant stresses are obtained via integration through the thickness using Equations (4.16) and (4.17).

4.3 Statics of a shell

All external loads are statically equivalent to a distributed resultant force and a resultant moment per unit area of the middle surface. The Cartesian components f^i of the resultant force are

$$f^i = Z^i_\beta f^\beta + f^3 N^i \tag{4.28}$$

where f^3 is the component in the normal direction of the resultant force. One requirement for obtaining the equations of equilibrium of a shell element is that the resultant force vanishes. Using the divergence theorem, one obtains, for the tangent plane,

$$\nabla_\alpha t^{\alpha\beta} - b^\beta_\alpha q^\alpha + f^\beta = 0 \tag{4.29}$$

where q^α is the shear force vector. For the normal direction,

$$\nabla_\alpha q^\alpha + b_{\alpha\beta} t^{\alpha\beta} + f^3 = 0 \tag{4.30}$$

These are the equations of equilibrium in the tangent plane (Equation (4.29)) and in the normal direction (Equation (4.30)). Another requirement is that the resultant moment vanishes. Finally, the equilibrium condition for the resultant moment is

$$\nabla_\alpha m^{\alpha\beta} - q^\beta = 0 \tag{4.31}$$

Then, from the resultant bending effort $m^{\alpha\beta}$ and the last equation, one can find the shear force vector q^α. Next, from the internal resultant forces $t^{\alpha\beta}$ and Equations (4.29) and (4.30), the final step is to find the Cartesian components of the resultant traction acting on the membrane, f^i.

Chapter 5

Numerical Technique: Spherical Harmonics Functions

Numerical methods for solving problems defined by partial differential equations can be classified into two categories: local and global. The widely used FEM is formulated in local terms, while the spectral method has global characteristics (Shen *et al.*, 2011). For complex geometries, FEM results are more suitable, while if the domain is flexible, spectral methods can provide better precision.

There are methods that combine the advantages of both approaches, e.g., the spectral-element method. In Wang and Dimitrakopoulos (2006), for example, a three-dimensional spectral boundary element algorithm for interfacial dynamics in a Stokes flow and/or gravity was presented. This approach exploits all the benefits of spectral methods along with the versatility of the FEM.

This work uses spherical harmonic functions to describe the strain and stress fields over the RBC surface. Using the formulations in the previous chapters, displacements and resultant efforts are calculated for the Gauss points. Then, by using spherical harmonic functions, these variables can be computed at any point on the surface. Therefore, it is an indirect method because it consists in calculating the coefficients of the harmonic analysis despite these coefficients not having any physical meaning.

5.1 Spectral methods

In the context of the numerical processes developed to solve partial differential equations, spectral methods belong to the class of weighted residual methods (WRMs). WRMs are based on a general method of obtaining solutions to equations of change (e.g., the en-

ergy balance equations for an incompressible fluid). The unknown solution is expanded in a set of trial functions, which are prespecified but are weighted by adjustable constants (or functions), which are chosen to yield the best solution to the differential equations (Finlayson, 1972).

The trial/test functions are a major feature that distinguishes spectral methods from the FEM or the finite difference method. In applications of spectral methods, global functions are used; trigonometric functions or orthogonal polynomials are commonly chosen.

5.2 Spherical harmonics

For smooth geometries, spectral methods can be used with great accuracy based on global arguments. In mathematics and the physical sciences, spherical harmonics are special functions defined on the surface of a sphere. They are often employed when solving partial differential equations that commonly occur in science. It is defined as a Galerkin formulation because the test functions are the same as the trial ones and it assumes that the boundary conditions are periodic or homogeneous.

Given a discrete function $f(\theta_i, \phi_j)$ defined on a grid with N latitudinal points (θ_i, $i = 1, ..., N$) and $2N-2$ longitudinal points (ϕ_j, $j = 1, ..., 2N-2$), a harmonic analysis consists of determining the coefficients $a_{m,n}$ and $b_{m,n}$ such that $f(\theta_i, \phi_j)$ can be synthesized as follows (Swarztrauber and Spotz, 2000):

$$f(\theta_i, \phi_j) = \sum_{n=0}^{N-1} \sum_{m=0}^{n} \bar{P}_n^m(\theta_i) \left(a_{m,n} \cos m\phi_j + b_{m,n} \sin m\phi_j\right) \tag{5.1}$$

where the $\bar{P}_n^m(\theta_i)$ are tabulations of the normalized associated Legendre functions, defined as:

$$\bar{P}_n^m(\theta) = \frac{1}{2^n n!} \left[\frac{2n+1}{2} \frac{(n-m)!}{(n+m!)}\right]^{1/2} \cos^m\theta \frac{d^{n+m}}{dx^{n+m}} \left(x^2-1\right)^n ; x = \sin\theta \tag{5.2}$$

Such an analysis consists of two phases. First, the fast Fourier transform is applied to compute

$$a_m(\theta_i) = \frac{1}{2N-2} \sum_{j=1}^{2N-2} f(\theta_i, \phi_j) \cos m\phi_j \tag{5.3}$$

and

$$b_m(\theta_i) = \frac{1}{2N-2} \sum_{j=1}^{2N-2} f(\theta_i, \phi_j) \sin m\phi_j \tag{5.4}$$

Using a Gaussian distribution for θ_i, the coefficients are then given in the second phase by

$$a_{m,n} = \sum_{i=1}^{N} w_i a_m(\theta_i) \bar{P}_n^m(\theta_i) \tag{5.5}$$

and

$$b_{m,n} = \sum_{i=1}^{N} w_i b_m(\theta_i) \bar{P}_n^m(\theta_i) \tag{5.6}$$

where the w_i are Gaussian weights. Once the coefficients are calculated the value of the function f can be computed at any point in the sphere surface using Equation (5.1)

The Gauss points are computed as the eigenvalues of a symmetric tridiagonal matrix, as described in Adams and Swarztrauber (1999), where the SPHEREPACK suite, which was used in this work, was introduced. SPHEREPACK is a collection of FORTRAN programs for harmonic transforms on Gaussian and equally spaced grids that can assist in the development of models for geophysical processes.

SPHEREPACK contains programs for computing certain common differential operators, such as divergence, vorticity, gradients, and the Laplacians of both scalar and vector functions. It can also be used to solve time-dependent partial differential equations. The accuracy is uniform on a sphere.

The subroutine `shagcm` computes the coefficients $a_{m,n}$ and $b_{m,n}$ to synthesize a given field. In this work, the subroutine `shagcm` was used to synthesize the following fields:

- normal vectors to the middle surface,
- strains (stretching and curvature),
- resultant moments and membrane efforts, and
- shear forces and traction on the middle surface.

These coefficients contain all the information of the given field; i.e., given $a_{m,n}$ and $b_{m,n}$, one can calculate the value of any of the mentioned fields at any point on the surface. For example, if X_i represents the geometry of an arbitrary state of the surface in Cartesian coordinates, then:

$$[a_{m,n}(X_i), b_{m,n}(X_i)] = \texttt{shagcm}(X_i) \tag{5.7}$$

synthesizes the field X_i. The subroutine `gradgcm` uses the coefficients $a_{m,n}$ and $b_{m,n}$ to calculate the basis of the middle surface $\mathbf{a}_1$ and $\mathbf{a}_1$ for both initial and deformed con-

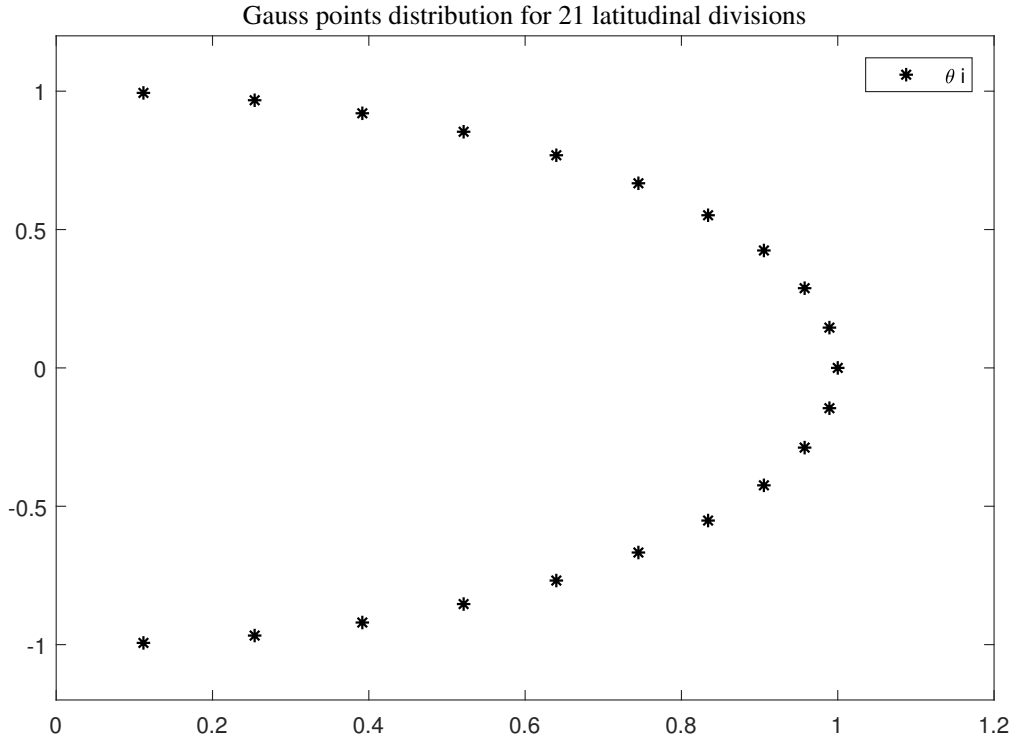

Figure 5.1: Gauss points distribution

figuration, i.e.

$$\left[\frac{\partial X_i}{\partial \theta}, \frac{\partial X_i}{\partial \phi}\right] = \texttt{gradcm}(a_{m,n}(X_i), b_{m,n}(X_i)) \tag{5.8}$$

The subroutine `gaqdm` is used to determine the latitudinal Gauss points and their respective weights for the desired latitudinal divisions. In Swarztrauber (2003), a full description of the calculation of the points and weights for Gauss-Legendre quadrature using double-precision computations is presented; thus, software implementations are highly robust.

Then, for a given latitude spacing of any surface that can be parameterized in spherical coordinates the subroutine `gaqdm` gives the distribution on the θ_i axis and their respective weights w_i. For a better understanding, take a number of latitudinal divisions of 21, $nlat = 21$, the distribution for a unit radius sphere on one longitudinal division is presented in Figure 5.1 and the values of θ_i with their respective weights w_i in Table 5.1

Table 5.1: Gauss points and weights

θ_i	w_i
0.1118	0.0160
0.2567	0.0370
0.4025	0.0571
0.5484	0.0761
0.6944	0.0934
0.8404	0.1088
0.9865	0.1218
1.1326	0.1323
1.2786	0.1399
1.4247	0.1445
1.5708	0.1461
1.7169	0.1445
1.8630	0.1399
2.0090	0.1323
2.1551	0.1218
2.3012	0.1088
2.4472	0.0934
2.5932	0.0761
2.7391	0.0571
2.8849	0.0370
3.0298	0.0160

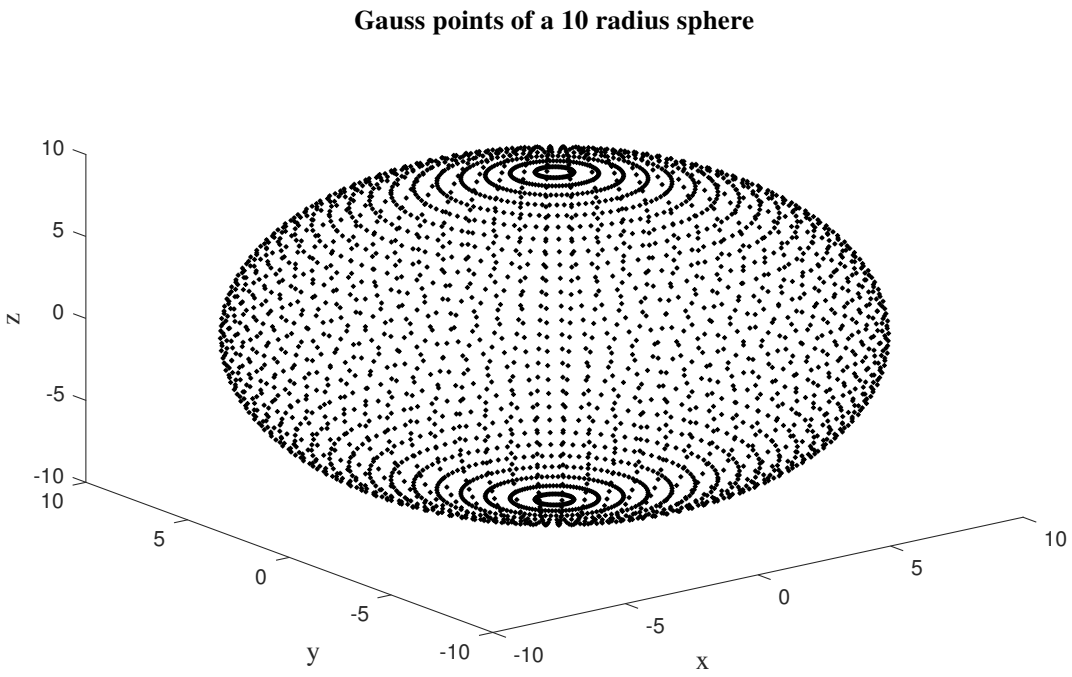

Figure 5.2: Gauss points of a 10 radius sphere

5.3 Implementation of the harmonic analysis

The computational implementation of the problem is as follow:

1. define the degree of the spherical harmonic expansion N in Equation (5.1);

2. define the latitude $nlat$ and longitude $nlon = 2(nlat-1)$ spacing that will determine the distribution of the Gauss points in the middle surface;

3. use the `gaqdm` routine to calculate the location of the Gauss points and create a mesh of this points;

4. get the initial sphere geometry using the parametric equations in Annex I for the mesh created. For a 10 radius sphere the Gauss points are shown in Figure 5.2;

5. get the deformed sphere geometry. For the inflation of a balloon example, the deformation is induced increasing the radius of the sphere. For the RBC the deformed geometry is flow induced;

6. calculate the basis vectors at each Gauss point using the `gradgcm` routine, then the normal vector is obtained as the cross product of the basis. This is done for the middle surface at the initial and deformed configuration;

7. get the metric $a_{\alpha\beta}$ and curvature $b_{\alpha\beta}$ tensors defined by Equation (3.15) and (3.20), respectively;

8. in this step the formulation described in section 3.4 is used, and the strain $\epsilon_{\alpha\beta}$ and bending tensor $\kappa_{\alpha\beta}$ of the motion are obtained;

9. integrate through the thickness direction, get the resultant membrane $t_{\alpha\beta}$ and bending $m_{\alpha\beta}$ stresses defined by Equation (4.16) and Equation (4.17) for each model described in section 4.1.1;

10. finally, get the resultant force f^i on each Gauss point of the middle surface using section 4.3.

Chapter 6

Numerical applications

In this chapter, the shell formulation presented in Chapter 3 is tested for the constitutive equations described in Chapter 4. Geometrically nonlinear analyses are performed.

6.1 Spherical balloon

With the aim of validating the code and evaluating shell deformations, in this example, the two strain functions defined in Equation (4.18) and Equation (4.19) are used to obtain the internal pressure defined in Equation (4.28). The inflation of a balloon consisting of an incompressible rubber is analyzed. A sketch of the internal pressure is shown in Figure 6.1.

The results are compared with Holzapfel (2000), in which the internal pressure and the circumferential stretch λ are given analytically. The initial radius of the rubber balloon is $R = 10.0$, and the wall thickness is $H = 0.1$. The shear modulus considered is $\mu = 4.225 \cdot 10^5$ N/m^2. For the Mooney-Rivlin model, $c_1 = 0.4375\mu$ and $c_2 = 0.0625\mu$. For the neo-Hookean model, $c_1 = \mu/2$.

The analytical expression

$$p = 2\frac{H}{R}\sum_{p=1}^{M}\mu_p\left(\lambda^{\alpha_p-3} - \lambda^{-2\alpha_p-3}\right) \tag{6.1}$$

gives the relation between the inflation pressure p_i and the circumferential stretch λ at any point on the rubber balloon for various constitutive models, here p is dimensionless. For the Mooney-Rivlin model, $\alpha_1 = 2$, $\alpha_2 = -2$ and $M = 2$; for the neo-Hookean model,

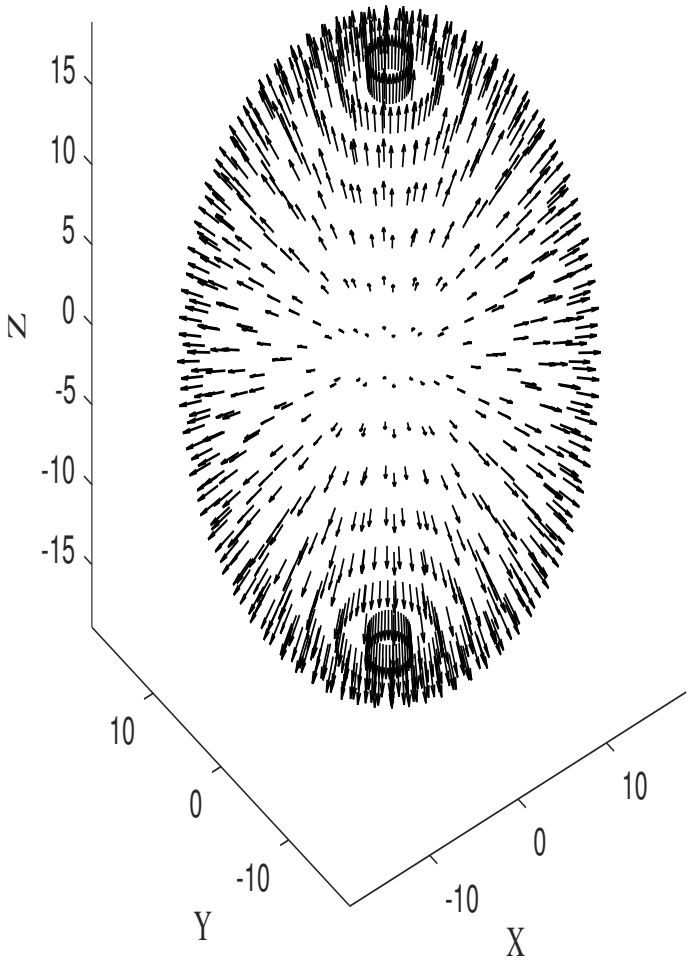

Figure 6.1: Internal pressure p

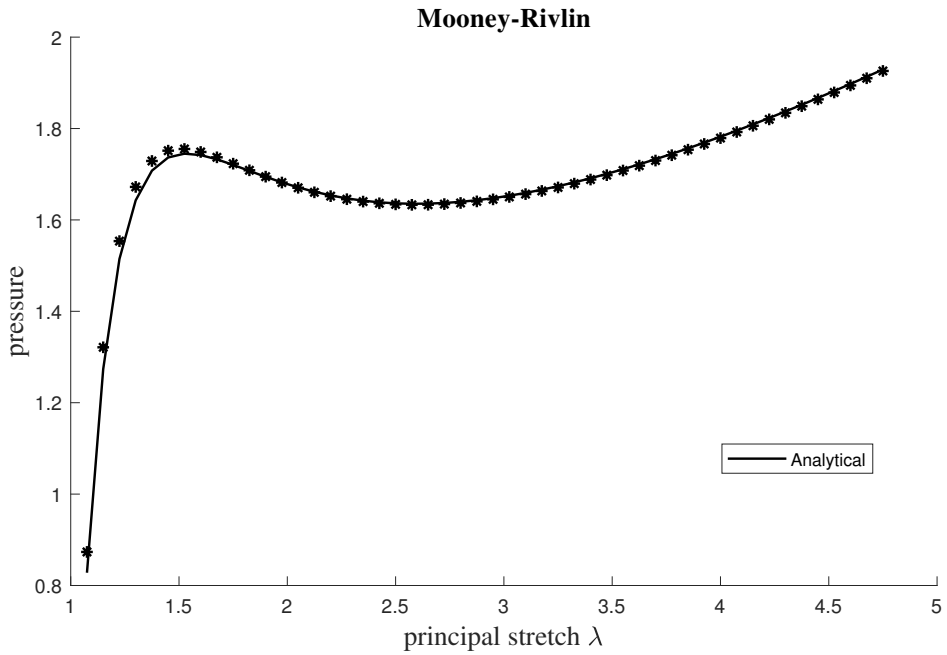

Figure 6.2: Inflation of a balloon: stretch-pressure curve

$\alpha_1 = 2$ and $M = 1$. That is, for the Mooney-Rivlin model:

$$p = 2\frac{H}{R}\left(\mu_1\left(\lambda^{-1} - \lambda^{-7}\right) + \mu_2\left(\lambda^{-5} - \lambda\right)\right) \tag{6.2}$$

and for the neo-Hookean:

$$p = 2\frac{H}{R}\mu\left(\lambda^{-1} - \lambda^{-7}\right) \tag{6.3}$$

Figure 6.2 shows the stretch-pressure curves for the Mooney-Rivlin model and figure 6.3 for the neo-Hookean model. Perfect agreement with the analytical solution is observed. The degree of the spherical harmonic expansion for undeformed and deformed shapes, used to compute the coefficients defined by Equation (5.5) and Equation (5.6), is $N = 10$. The implemented formulations result in low-cost and robust computations. Figure 6.4 shows the undeformed geometry as a full spheroid and the deformed geometries at every other load step as half-spheroids.

The analytical expression

$$\sigma = \sum_{p=1}^{M} \mu_p\left(\lambda^{\alpha_p} - \lambda^{-2\alpha_p}\right) \tag{6.4}$$

gives the expression for the true axial stress σ as function of the stretch. Good agreement

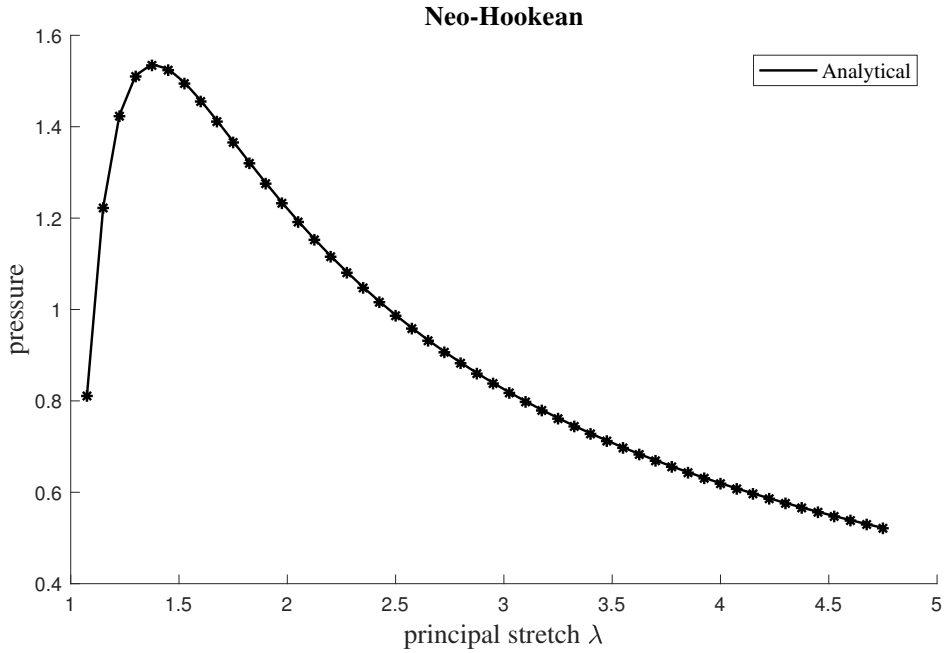

Figure 6.3: Inflation of a balloon: stretch-pressure curve

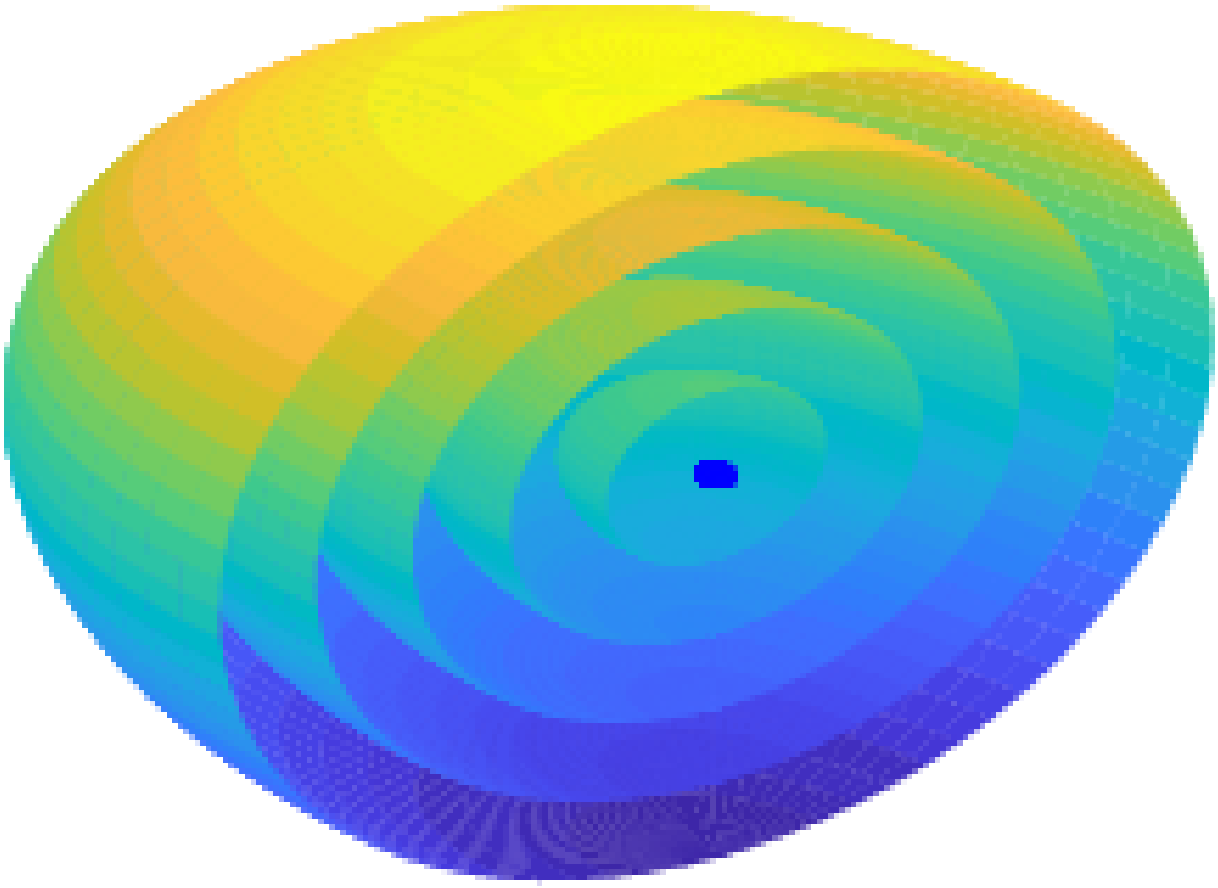

Figure 6.4: Inflation of a balloon: undeformed and deformed geometries

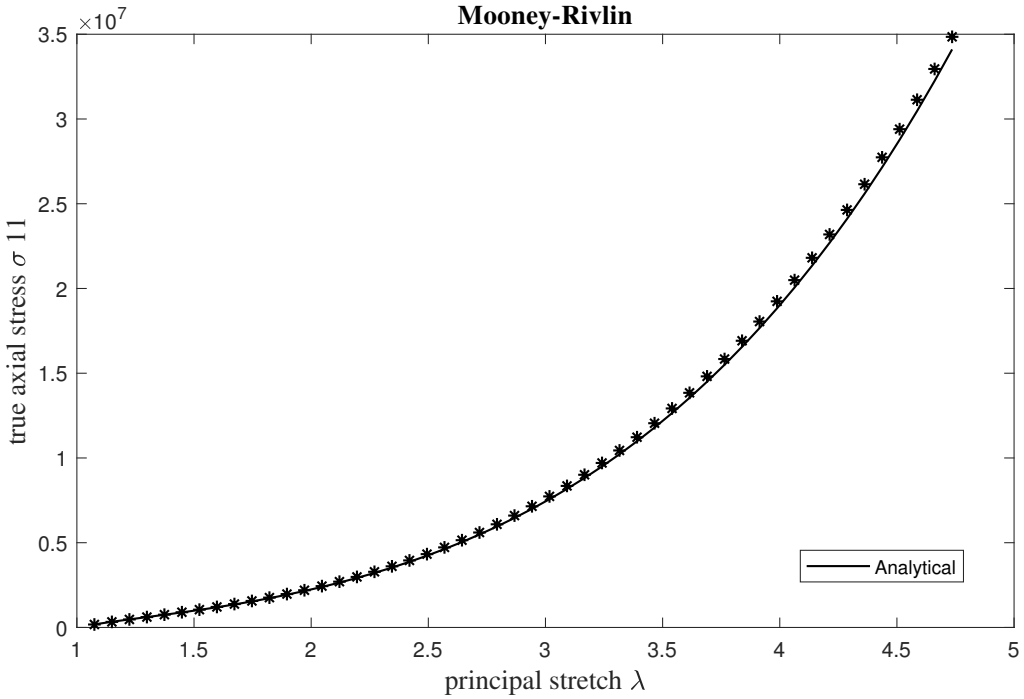

Figure 6.5: Inflation of a balloon: stretch-stress curve

is shown in figure 6.5 and figure 6.6 for the Mooney-Rivlin and Neo-Hookean models, respectively.

To determine the proper grid for the simulation, an analysis of convergence was performed as shown in Figure 6.7, therefore, the value of $nlat = 41$ was used for the analysis made in this example.

This numerical test is largely studied, in addition to the cited references it also was performed and can be found in Needleman (1977), Wriggers and Taylor (1990), Gruttmann and Taylor (1992), Ibrahimbegović and Gruttmann (1993) and Moita (1994). The latter used a three-dimensional non-linear membrane element, deriving the finite element equations for the element using a total Lagrangian formulation. As the problem exhibits a Snap-through and to pass this limit-point an arc-length procedure was applied in addition to the full Newton-Raphson method to determine the complete solution path. Using approximately six iterations per step with a quadratic convergence behaviour.

More recently, Kiendl *et al.* (2015) studied the same problem using a Non-Uniform Rational B-Splines discretization of the sphere geometry and they found a perfect agreement with the analytical solutions. Since this example has been widely studied it is a benchmark problem in the study of hyperelastic materials. In this work, with the formu-

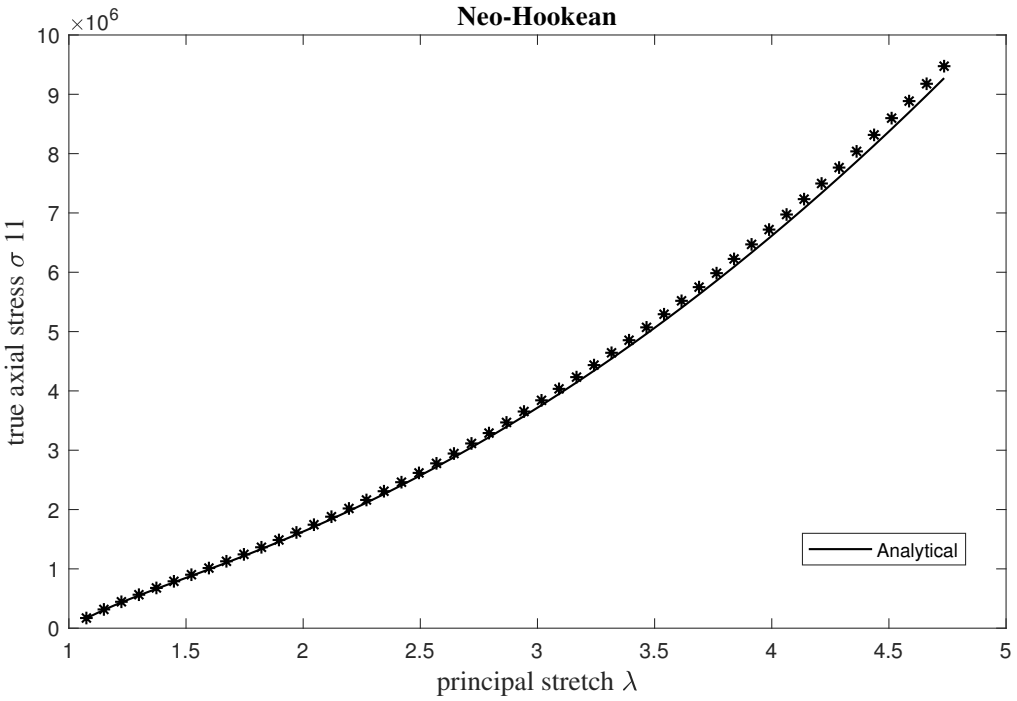

Figure 6.6: Inflation of a balloon: stretch-stress curve

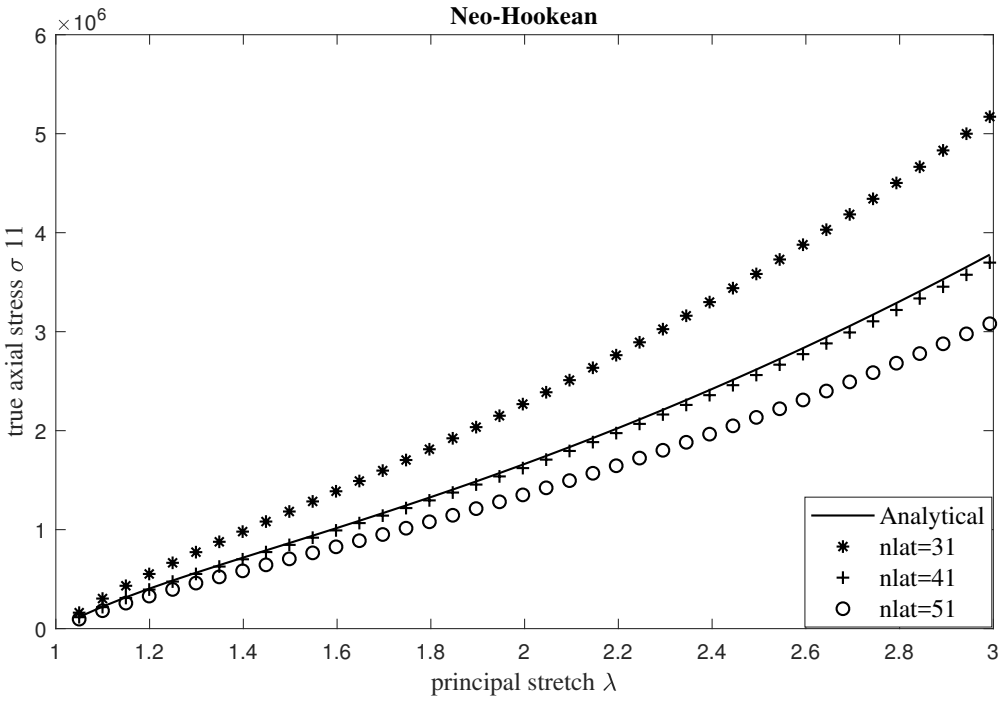

Figure 6.7: Inflation of a balloon: stretch-stress curves varying nlat

lation presented and using a spherical harmonic analysis, not found in literature a perfect agreement with the analytical expressions are found. The code developed deals whit high nonlinearities without any convergence problem.

6.2 RBC simulations in an infinite shear flow

For this implementation, the deformation of a solitary RBC suspended in an infinite shear flow along the x-axis is analyzed. The study of the flow was not part of this work; the main focus was the kinematics, the constitutive relations for a second-order analysis and the use of spherical harmonic functions.

The fluid and solid mechanics is coupled from the continuity of velocities between the liquids and the membrane. The fluid mechanics is described by the Stokes equations because the size of the particle is very small. Thus, the inertial effects may be neglected. To calculate the velocity on a point that lies in the cell membrane, the boundary-integral formulation for Stokes flow must be solved (Pozrikidis, 1992).

Under the assumption of an unstressed initial state, a normal RBC has the shape of a biconcave disk. The following parametric equations are used to describe a resting RBC Pozrikidis (2005):

$$\begin{gathered} x_1 = \alpha \sin\phi \cos\theta \\ x_2 = \alpha \sin\phi \sin\theta \\ x_3 = a\tfrac{\alpha}{2}\left(0.207 + 2.003\sin^2\phi - 1.123\sin^4\phi\right)\cos\phi \\ 0 \leq \theta \leq 2\pi \\ 0 \leq \phi \leq \pi \end{gathered} \tag{6.5}$$

where the dimensionless coefficient $\alpha = 1.3858189$ is the ratio of the maximum radius of the biconcave disk to the equivalent cell radius a; for a normal RBC, $a \approx 2.82$ μm. The resting shape is shown in Figure 6.8 and Figure 6.9

A sketch of an undeformed biconcave red cell suspended in a simple shear flow is shown in Figure 6.10. The Kelvin-Voigth model is used. The elastic part of the stress tensor is modeled as a neo-Hookean material with $\mu = 3\text{x}10^{-3} dyn/\mu m$ (Pozrikidis, 2005) and for the membrane viscosity $\mu^s = 5\text{x}10^{-4} dyn/\mu m$ (Barthes-Biesel and Sgaier, 1985).

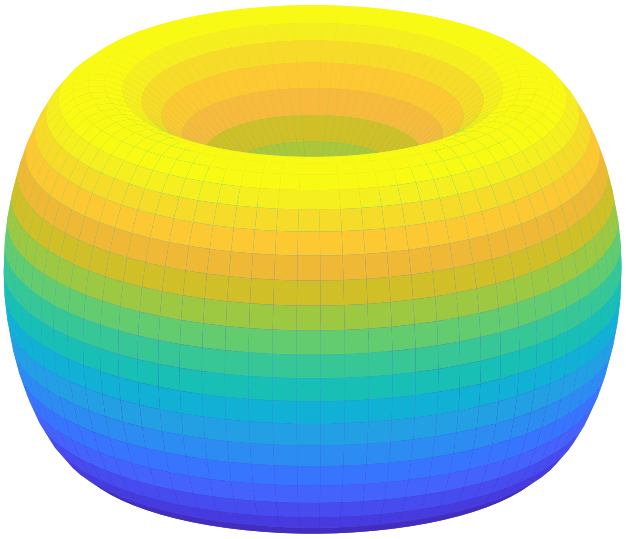

Figure 6.8: Undeformed RBC

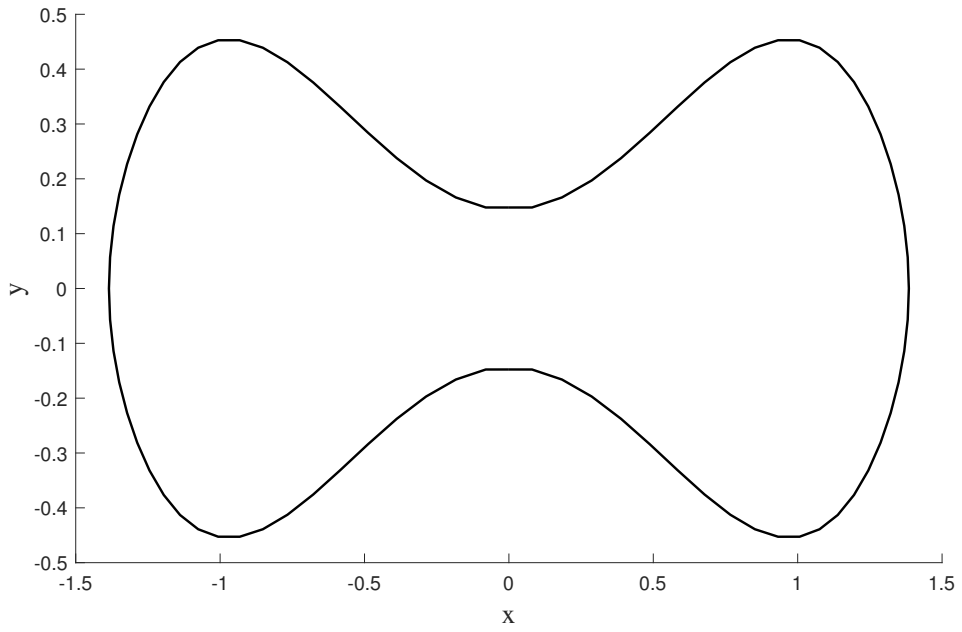

Figure 6.9: Sketch of an undeformed RBC

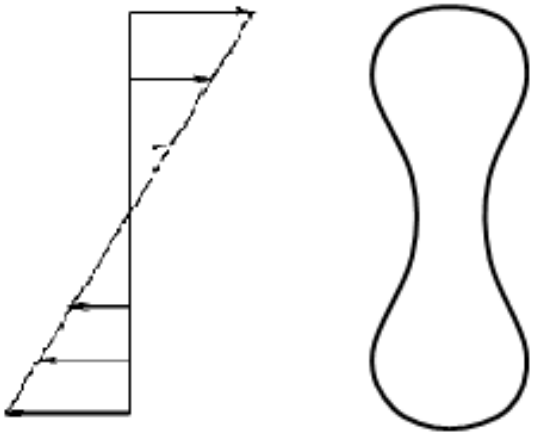

Figure 6.10: Sketch of an undeformed RBC suspended in a simple shear flow

Experimental data have shown that a suspension of human RBCs moving through glass tubes deform into a parachute shape as shown in Pozrikidis (2005) (Figure 6.11). Figure 6.12 and Figure 6.13 shows the evolution of the RBC from a resting shape rotated $\pi/2$ ending in a parachute shape por $n = 200$ steps each of $\Delta t = 1e - 2$.

In order to evaluate the contribution of the viscous part, two analysis of 10000 steps with $\Delta t = 1e - 3$ are made from a resting shape rotated $\pi/4$. In the first one only the elastic contribution is considered using the neo-Hooken model. Then, the viscous part is added to the elastic part for the Kelvin-Voigth model. The evolution of the resultant traction vs. the stretch of a Gauss point is shown in Figure 6.14. The contribution of the viscous part seems not to be significant. This could be for the chosen parameters, a deeper study of the parameters must be done in further works. The position of the Gauss points for the resting shape is shown in Figure 6.15 where the Gauss point analyzed is highlighted.

From Figure 6.16 to Figure 6.26 the evolution of a RBC from a unstressed state $n = 1$ to $n = 10000$ for a $\Delta t = 1e - 3$ is shown as well as the resultant traction in the surface for the flow-induced deformation. Showing the capacity of the developed algorithm in leading with flow-structure interaction for large strains.

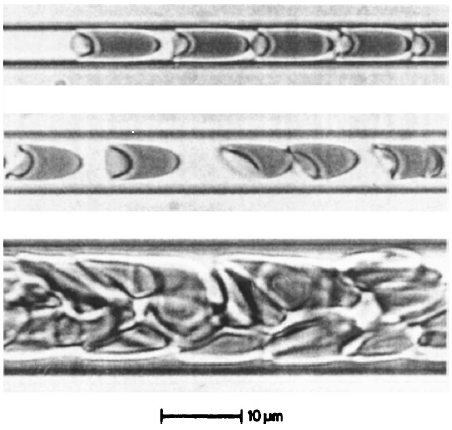

Figure 6.11: From Pozrikidis (2005). A suspension of human RBCs moving through glass tubes with approximate diameters 4.5 μm (top), 7 μm (middle), and 15 μm (bottom); the flow direction is from left to right.

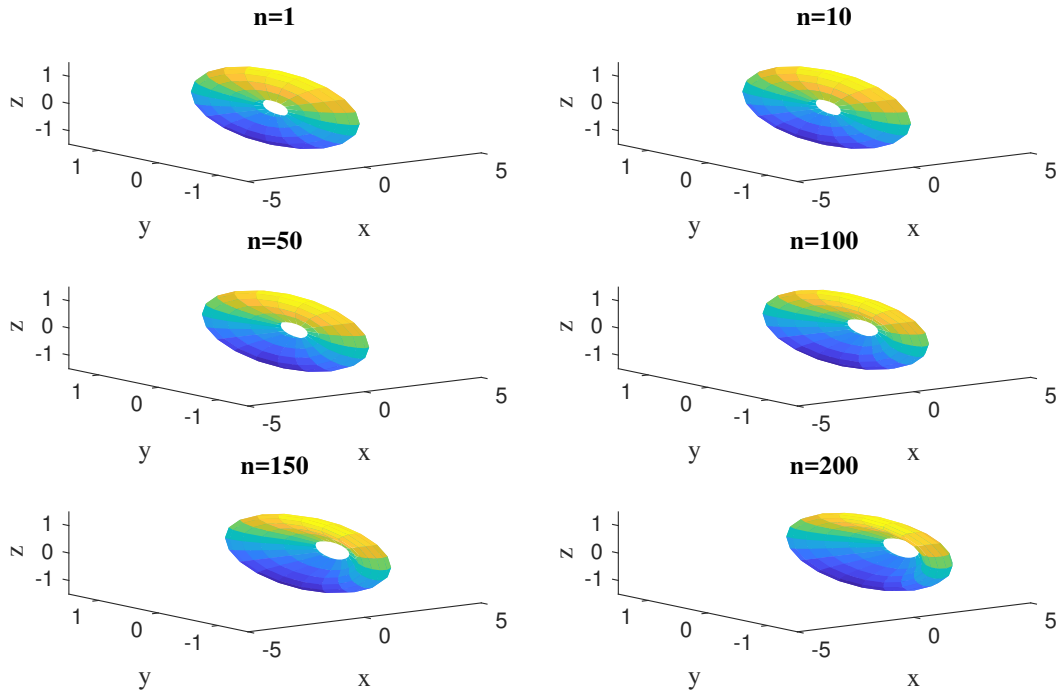

Figure 6.12: Snapshots of a RBC in a simple shear flow

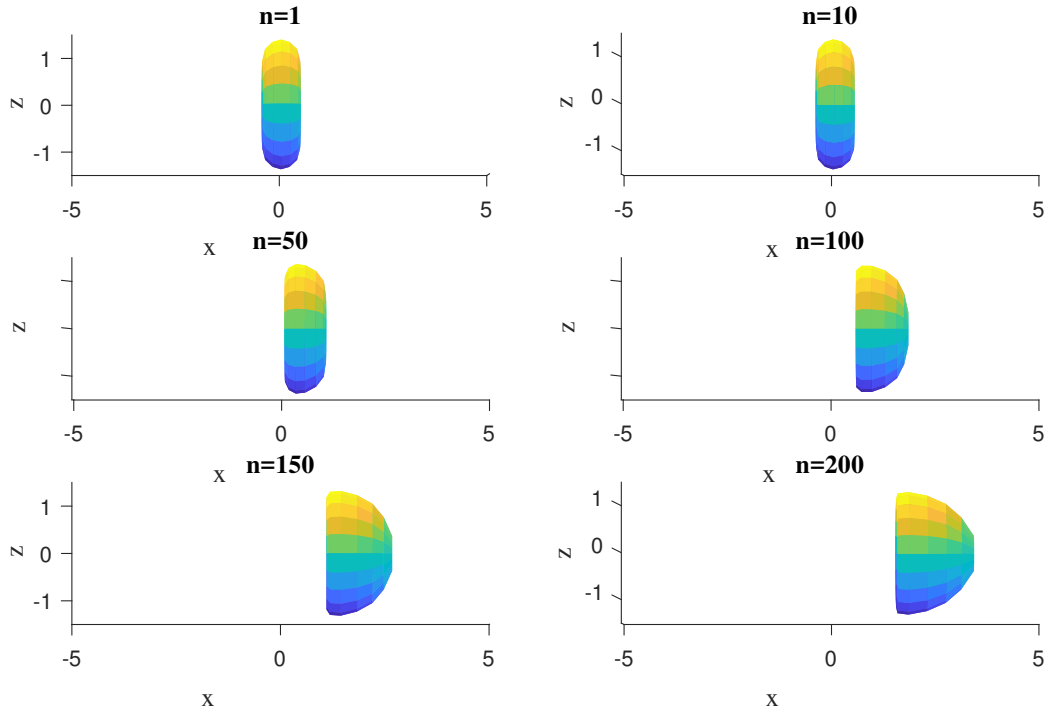

Figure 6.13: Snapshots of a RBC in a simple shear flow

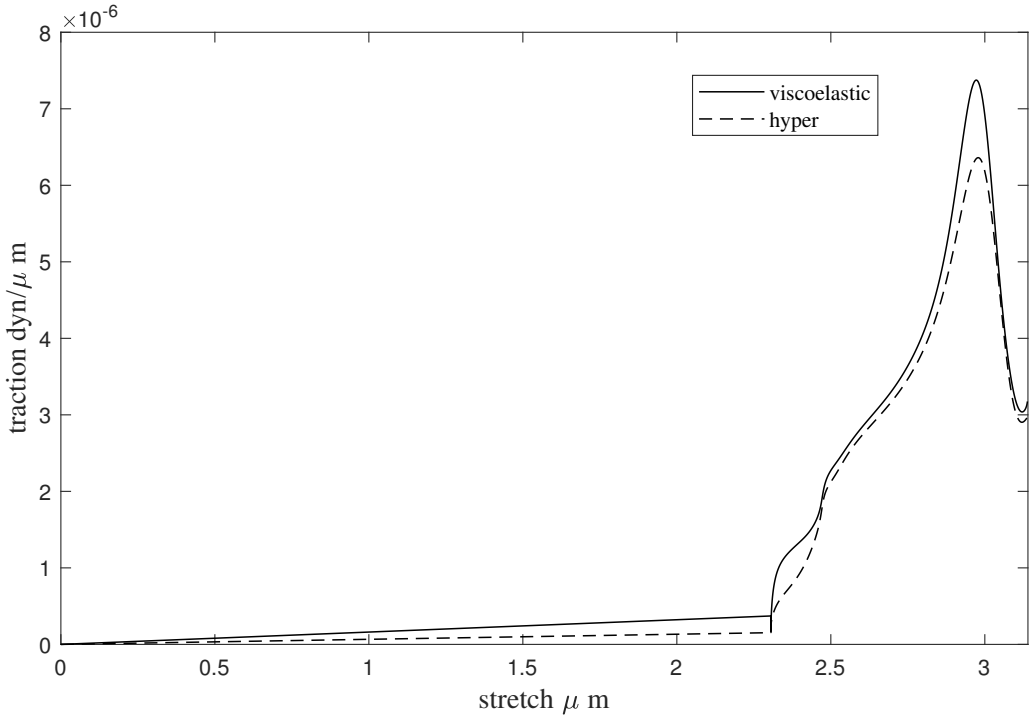

Figure 6.14: Resultant traction vs. Stretch for the viscoelastic and hyperelastic models

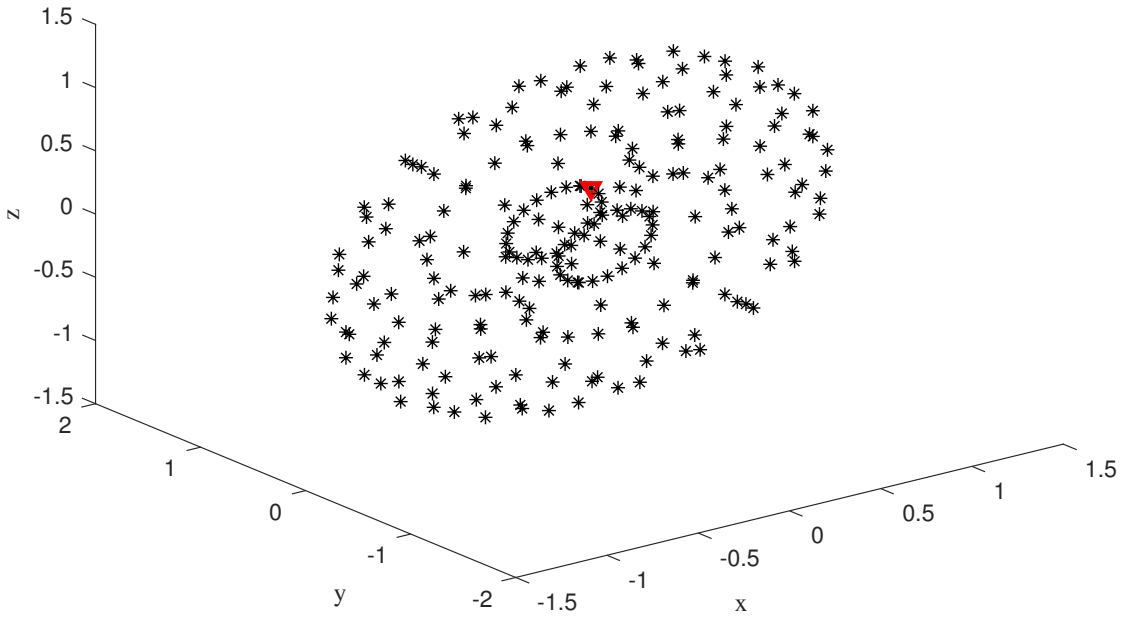

Figure 6.15: Position of the Gauss points for the resting RBC

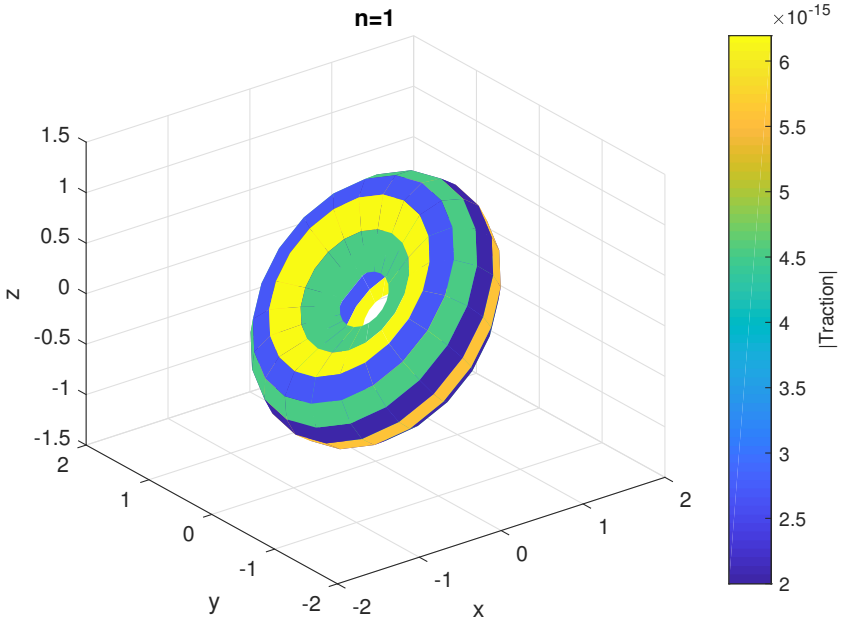

Figure 6.16: Snapshot of a RBC in a simple shear flow. $step = 1$

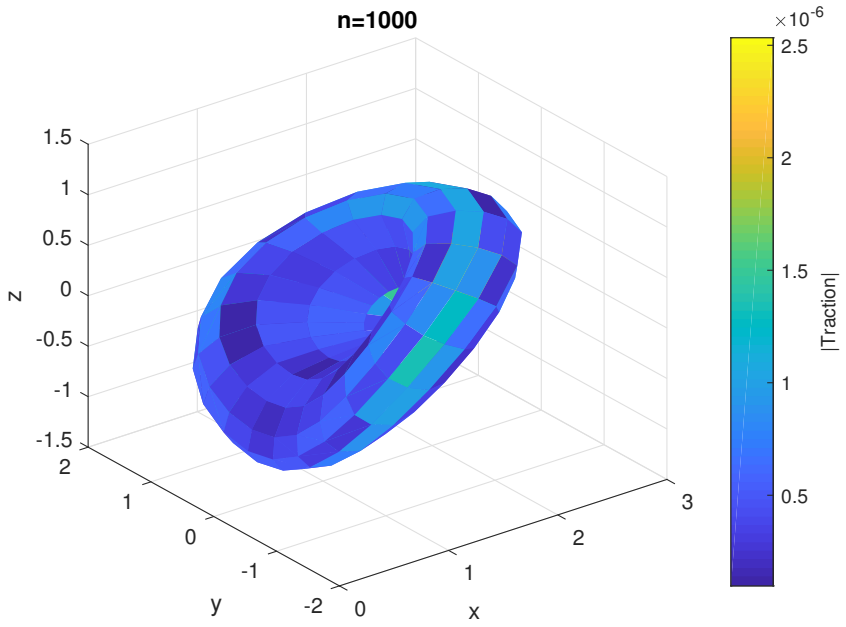

Figure 6.17: Snapshot of a RBC in a simple shear flow. $step = 1000$

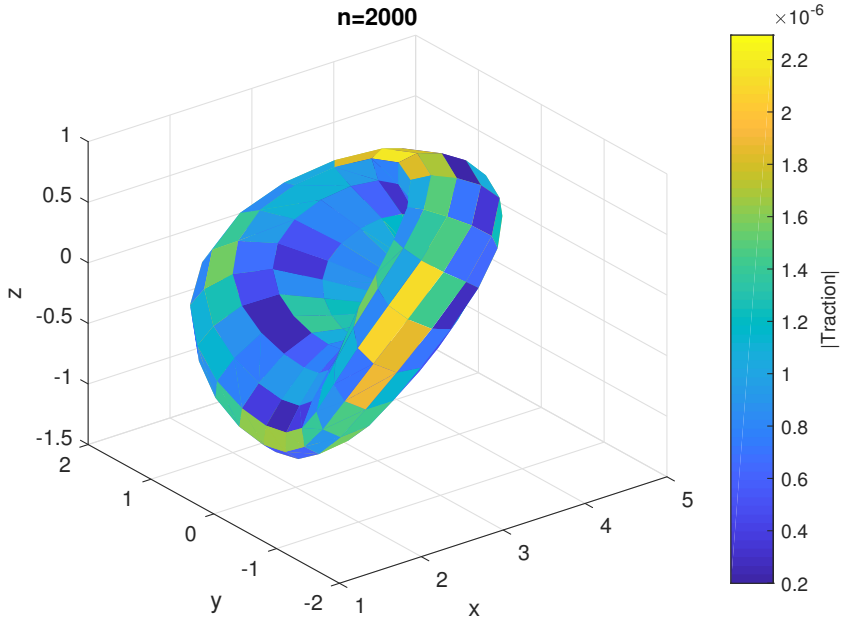

Figure 6.18: Snapshot of a RBC in a simple shear flow. $step = 2000$

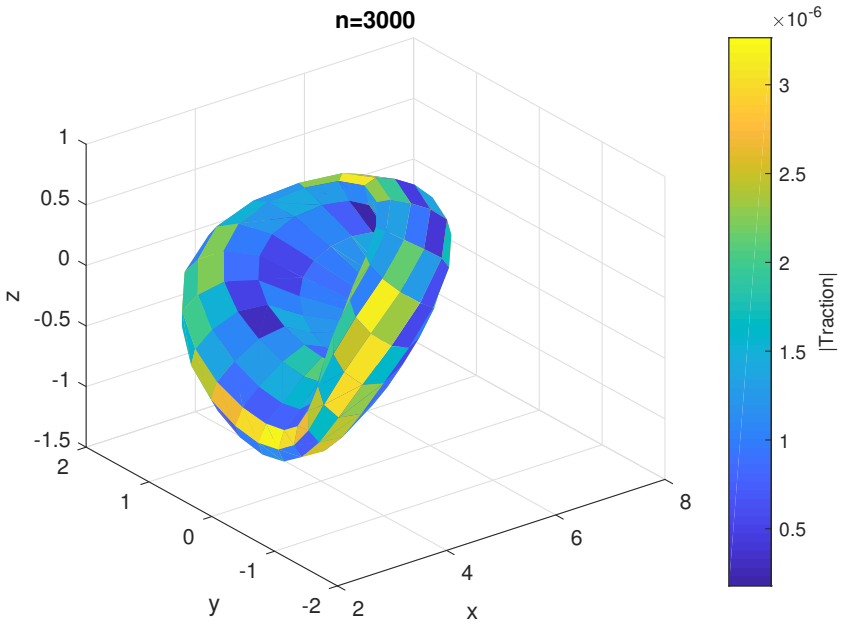

Figure 6.19: Snapshot of a RBC in a simple shear flow. $step = 3000$

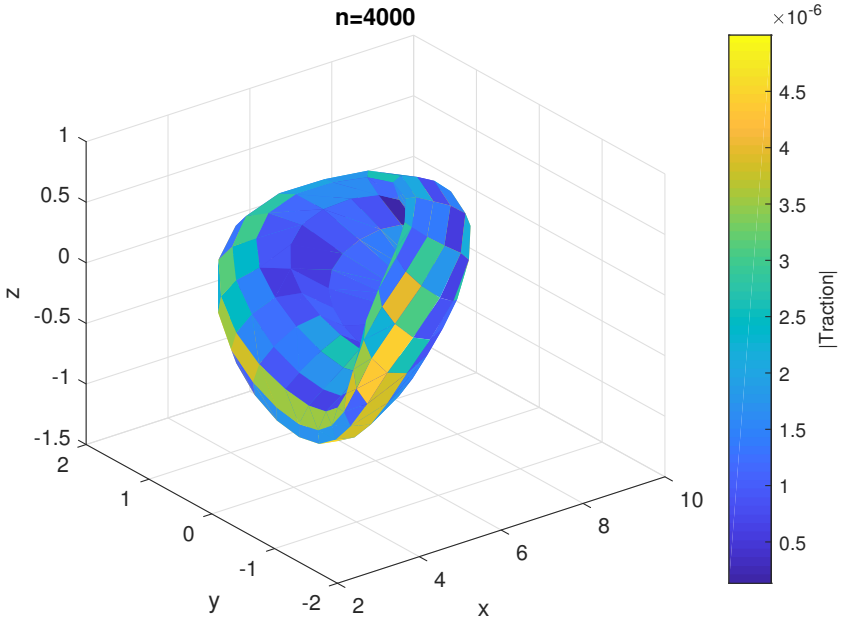

Figure 6.20: Snapshot of a RBC in a simple shear flow. $step = 4000$

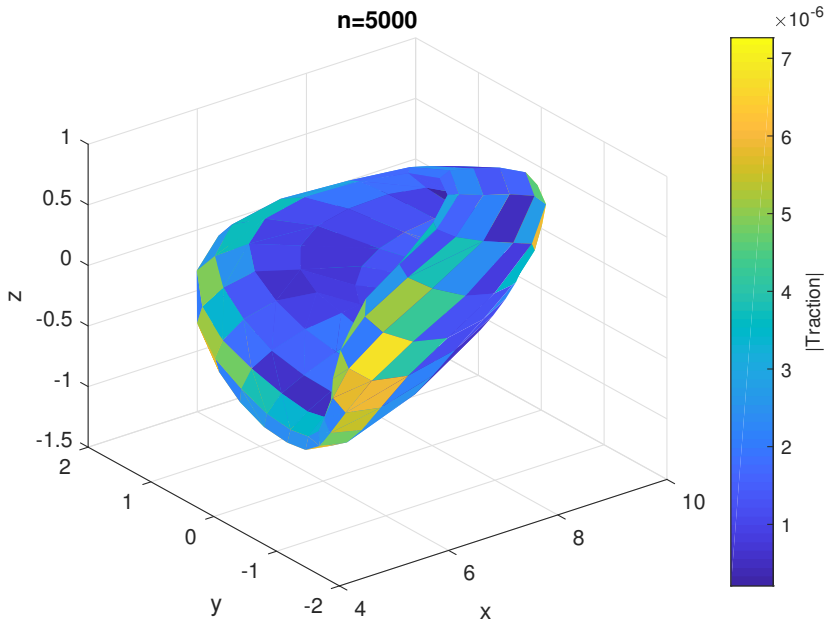

Figure 6.21: Snapshot of a RBC in a simple shear flow. $step = 5000$

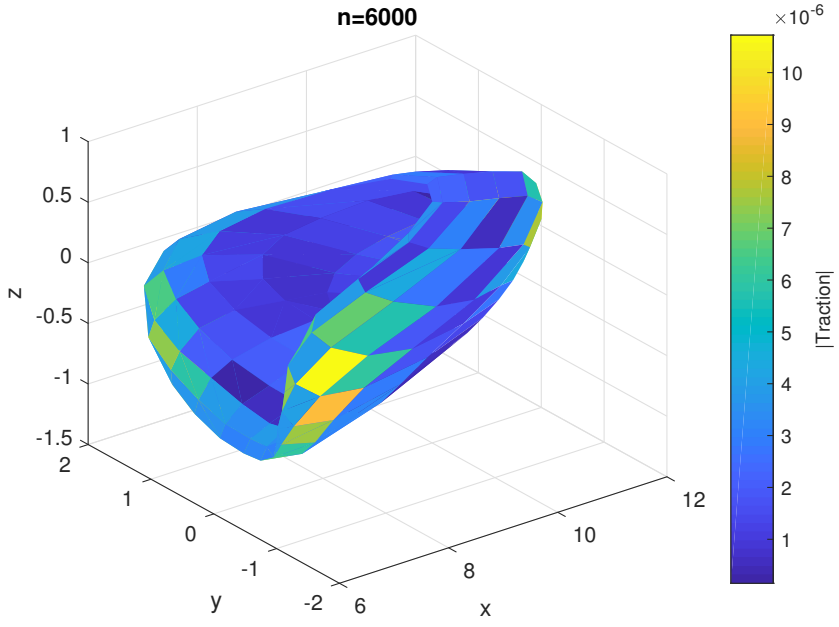

Figure 6.22: Snapshot of a RBC in a simple shear flow. $step = 6000$

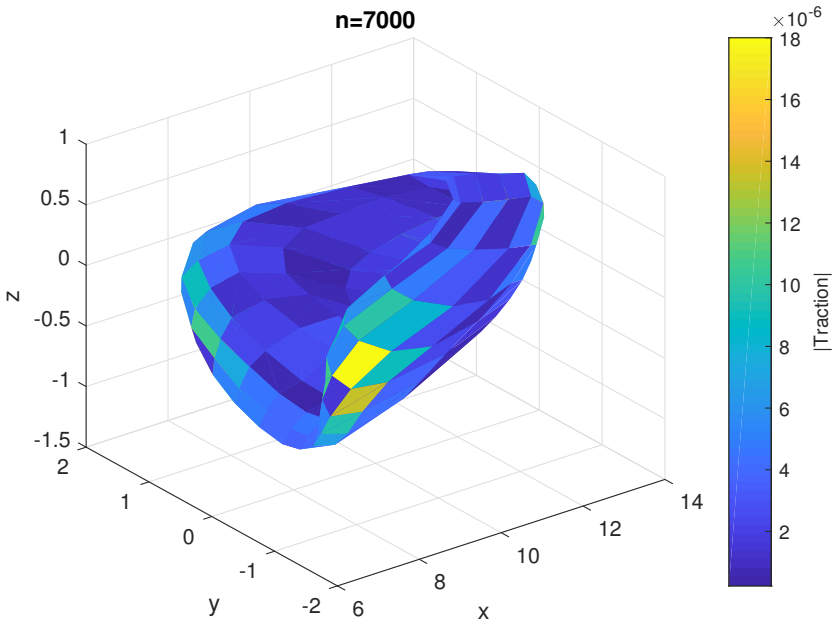

Figure 6.23: Snapshot of a RBC in a simple shear flow. $step = 7000$

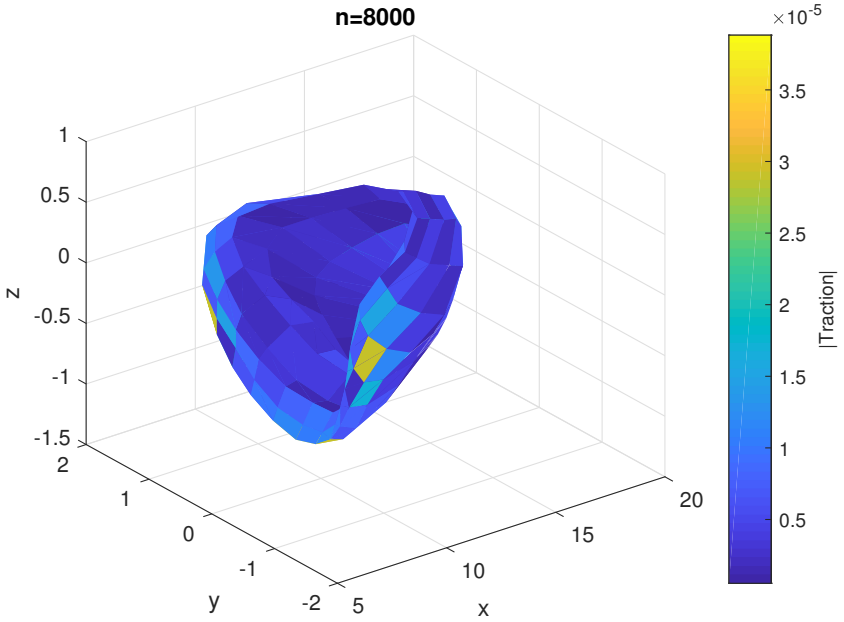

Figure 6.24: Snapshot of a RBC in a simple shear flow. $step = 8000$

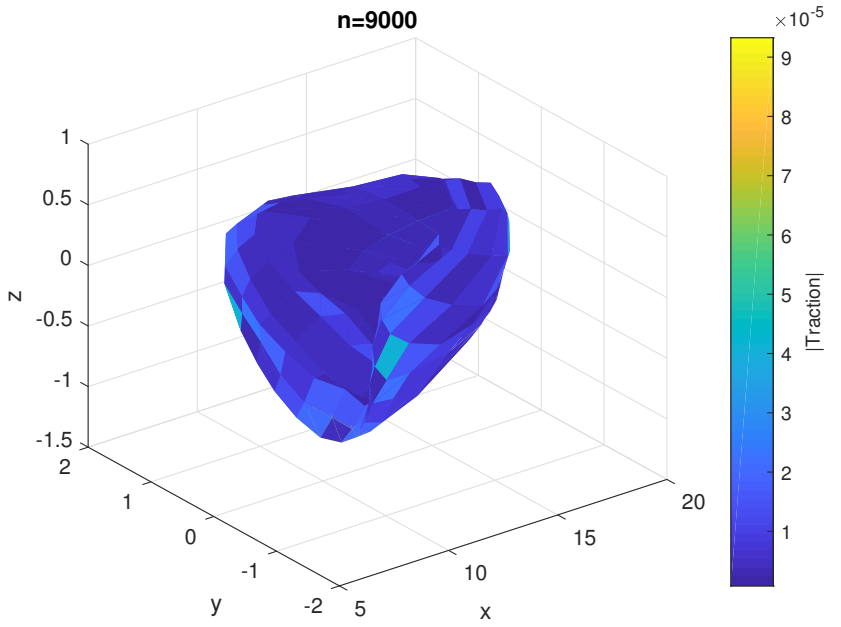

Figure 6.25: Snapshot of a RBC in a simple shear flow. $step = 9000$

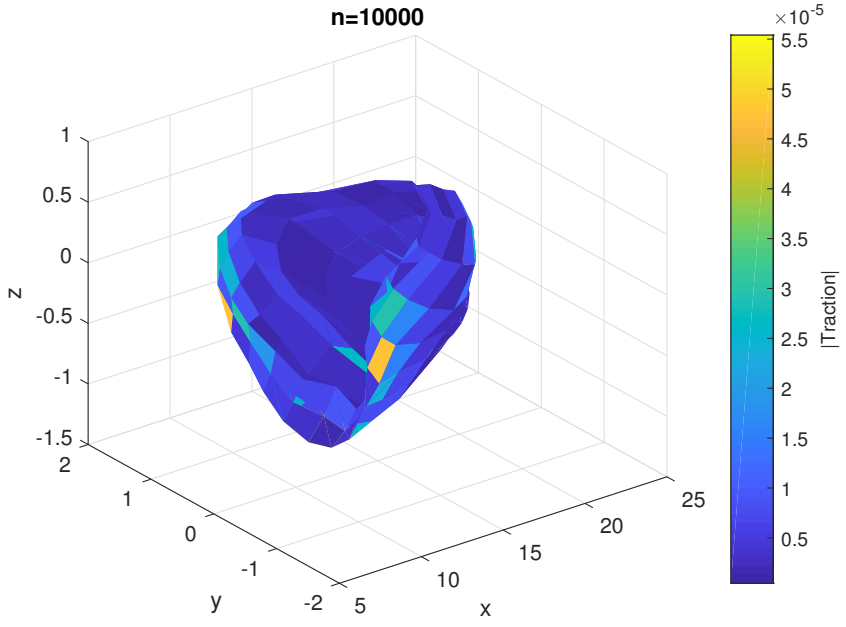

Figure 6.26: Snapshot of a RBC in a simple shear flow. $step = 10000$

Chapter 7

Conclusions

7.1 General conclusions

This work focused on the study of second-order analyses with the aim of modeling biological cells. The ultimate goal is to use the classical shell theory to study the nonlinear behavior of the RBC membrane. There are several difficulties that can arise when dealing with highly nonlinear analyses. Large deformations and nonlinear constitutive relations can lead to numerical instabilities, depending on the numerical method used.

The use of tensor calculus facilitated the kinematic description and the formulation of the constitutive relations of the material, allowing calculations to be performed in several coordinate systems via simple transformations. Thus, by means of the dimensional reduction achieved through the Kirchhoff hypotheses, the stresses, deformations, etc. were calculated in 2D space, and using the fundamental tensors and the shift tensor, these values were simply transformed into Cartesian coordinates.

The neo-Hookean and Rivlin-Mooney hyperelastic constitutive models were considered for simulating large elastic deformations, and no problems were observed. The incompressibility condition was imposed, and the resultant membrane and bending efforts were calculated. In the development of the thin shell elements, a Lagrangian description was used, and when this description was implemented, the results showed excellent congruence with analytical expressions found in the literature.

Because the geometry of RBCs can be described in spherical coordinates, spherical harmonic functions were used to synthesize the main analysis variables. Fields of resultant efforts such as traction and bending, strains, curvature, fundamental tensors, and normal

vectors at the surface were synthesized based on the coefficients $a_{n,m}$ and $b_{n,m}$.

These coefficients store the information of any tensor fields, allowing their values at any location on the surface to be known. This is the main reason why the developed code has a low computational cost, even when dealing with large nonlinearities. It is important to note that this work was based on a indirect method because it consists in calculating the coefficients of the harmonic analysis despite these coefficients not having any physical meaning.

The main advantage found during the development of this work is the fact that there is no need for an iteration process in the calculation of the fields (stresses, strains) because it is a semi-analytical method. Thus, using the classical shell theory, these fields can be computed in a grid of Gauss points.

Whereas it is established that the RBC membrane do have a viscous component, in the comparison made between the purely hyperelastic models and the model considering a viscous contribution, no significant contribution of the membrane viscosity was noted. This may come about as a result of the parameters adopted both for the membrane and for the fluid. So a parametric analysis is highly recommended as next step, besides the Kelvin-Voigth model, considered in this work, is likely not able to reproduce the exact behavior of the RBC membrane.

As mentioned before, this work belongs to a project that is still in its early stages thus, many limitations can be mentioned so far. In the development of this work the following were some of the major findings

- The geometry must be closed and should be described in spherical coordinates. This is also the main feature of the method used in this work, because that is exactly why this approach was studied as the geometry of the RBCs can be defined in spherical coordinates even though this restricts its applications to other geometries.
- The study of contact between several RBCs should be more challenging than the simulations presented in this work due to the nonlinearity result of the friction between cells.
- Given that the harmonic analysis synthesizes a field over a sphere, the formulation presented here only considers surface loads.

7.2 Future Works

This work was part of the beginning of a research project with a very ambitious goal: the modeling of RBCs passing through microcapillaries. Thus, the need for further work corresponds to the continuation of the project itself. The following may be mentioned as suggestions for future work:

- in this work the deformed configuration was imposed in order to obtain the resulting efforts. Thus, implement the calculation of the deformed configuration given an specific field of traction over the surface is a natural next step;
- modeling specific experiments such as the optical tweezers method, with the aim of numerically validating the presented viscoelastic model;
- studying the interaction of several RBCs in a confined blood flow;
- implementing the tank-treading motion in a shear flow;
- implementing the contact between the cells and the walls of the microcapillaries;
- studying other methods of introducing the viscous part of the Kelvin-Voigt model, for example, through a time-dependent function for the relaxation of the membrane shear viscosity. Also, a spatial formulation can be developed to study if there is any difference with the formulation presented ;
- studying the behavior of unhealthy RBCs; and
- studying the influence of the parameters from the constitutive models proposed in this work.

Bibliography

ABDALLAH, N., DEGOND, P., MARKOWICH, P. and SCHMEISER, C. (2001). High field approximations of the spherical harmonics expansion model for semiconductors. Zeitschrift fur Angewandte Mathematik und Physik, 52 (2): 201–230. 16

ABDOLALI, F., ZOROOFI, R. A., OTAKE, Y. and SATO, Y. (2017). Automated classification of maxillofacial cysts in cone beam CT images using contourlet transformation and Spherical Harmonics. Computer methods and programs in biomedicine, 139: 197–207. 14

ADAMS, J. C. and SWARZTRAUBER, P. N. (1999). SPHEREPACK 3.0: A model development facility. Monthly Weather Review, 127 (8): 1872–1878. 40

ALLU, P. and MAZUMDER, S. (2016). Hybrid ballistic–diffusive solution to the frequency-dependent phonon Boltzmann transport equation. International Journal of Heat and Mass Transfer, 100: 165–177. 19

ALLU, P. and MAZUMDER, S. (2018). Comparative assessment of deterministic approaches to modeling quasi-ballistic phonon heat conduction in multi-dimensional geometry. International Journal of Thermal Sciences, 127: 181–193. 18

AYARI, R., ABDALLAH, A. B., SFAR, R., GHORBEL, F. and BEDOUI, M. H. (2014). Analysis of regional deformation of the heart's left ventricle using invariant SPHARM descriptors. IRBM, 35 (5): 226–232. 13

BARTHES-BIESEL, D. and SGAIER, H. (1985). Role of membrane viscosity in the orientation and deformation of a spherical capsule suspended in shear flow. Journal of Fluid Mechanics, 160: 119–135. 9, 36, 51

BONET, J., GIL, A. J. and WOOD, R. D. (2016). Nonlinear Solid Mechanics for Finite Element Analysis: Statics. Cambridge University Press. 35

BRIARD, A., GRÉA, B.-J., MONS, V., CAMBON, C., GOMEZ, T. and SAGAUT, P. (2018). Advanced spectral anisotropic modelling for shear flows. Journal of Turbulence, 19 (7): 570–599. 20

CAMMAROTA, V., MARINUCCI, D. and WIGMAN, I. (2016). Fluctuations of the Euler-Poincare Characteristic for random Spherical Harmonics. Proceeding of the American Mathematical Society, 144 (11): 4759–4775. 17

CAMPESE, S., MARINUCCI, D. and ROSSI, M. (2018). Approximate normality of high-energy hyperspherical eigenfunctions. Journal of Mathematical Analysis and Applications, 461 (1): 500–522. 17

CASQUERO, H., BONA-CASAS, C. and GOMEZ, H. (2017). NURBS-based numerical proxies for red blood cells and circulating tumor cells in microscale blood flow. Computer Methods in Applied Mechanics and Engineering, 316: 646 – 667, special Issue on Isogeometric Analysis: Progress and Challenges.
URL http://www.sciencedirect.com/science/article/pii/S0045782516312233 8

CHEE, C., LEE, H. and LU, C. (2008). Using 3D fluid–structure interaction model to analyse the biomechanical properties of erythrocyte. Physics Letters A, 372 (9): 1357 – 1362.
URL http://www.sciencedirect.com/science/article/pii/S0375960107013709 8

CHEN, W. (2000). Stress distribution in a rotating elastic functionally graded material hollow sphere with spherical isotropy. The Journal of Strain Analysis for Engineering Design, 35 (1): 13–20. 20

CHEN, X., SUN, F., YANG, D., REN, S., ZHANG, Q. and LIANG, J. (2015). Hybrid simplified spherical harmonics with diffusion equation for light propagation in tissues. Physics in Medicine & Biology, 60 (16): 6305. 13

CHENG, L., XIA, X., YU, W., SCRIVEN, L. and GERBERICH, W. (2000). Flat-punch indentation of viscoelastic material. Journal of Polymer Science Part B: Polymer Physics, 38 (1): 10–22. 7

CHENG, Z. and SHI, Z. (2018). Composite periodic foundation and its application for seismic isolation. Earthquake Engineering & Structural Dynamics, 47 (4): 925–944. 10

CHU, M., VISHWANATH, K., KLOSE, A. D. and DEHGHANI, H. (2009). Light transport in biological tissue using three-dimensional frequency-domain simplified spherical harmonics equations. Physics in Medicine & Biology, 54 (8): 2493. 14

DAI, F., FENG, H. and TIKHONOV, S. (2016). Reverse Holder's Inequality for Spherical Harmonics. Proceeding of the American Mathematical Society, 144 (3): 1041–1051. 17

DAO, M., LIM, C. and SURESH, S. (2003). Mechanics of the human red blood cell deformed by optical tweezers. Journal of the Mechanics and Physics of Solids, 51 (11): 2259 – 2280, proceedings of a Symposium on Dynamic Failure and Thin Film Mechanics, honoring Professor L.B. Freund. 7

DEGOND, P. and SCHMEISER, C. (1999). Kinetic boundary layers and fluid-kinetic coupling in semiconductors. Transport Theory and Statistical Physics, 28 (1): 31–55. 16

DEGOND, P. and ZHANG, K. (2002). Diffusion approximation of a scattering matrix model of a semiconductor superlattice. Siam Journal of Applied Mathematics, 63 (1): 279–298. 16

DIAZ, A., BARTHèS-BIESEL, D. and PELEKASIS, N. (2001). Effect of membrane viscosity on the dynamic response of an axisymmetric capsule. Physics of Fluids, 13 (12): 3835–3838. 9

DODDI, S. K. and BAGCHI, P. (2008). Lateral migration of a capsule in a plane Poiseuille flow in a channel. International Journal of Multiphase Flow, 34 (10): 966 – 986. 8

DOLGOV, V. Y., KLYSHNIKOV, K. Y., OVCHARENKO, E. A., GLUSHKOVA, T. V., BATRANIN, A. V., AGIENKO, A. S., KUDRYAVTSEVA, Y. A., YUZHALIN, A. E. and KUTIKHIN, A. G. (2019). Finite Element Analysis-Based Approach for Prediction of Aneurysm-Prone Arterial Segments. Journal of Medical and Biological Engineering, 39 (1): 102–108.
URL https://doi.org/10.1007/s40846-018-0422-x 1

DONG, C., SKALAK, R. and SUNG, K.-L. P. (1991). Cytoplasmic rheology of passive neutrophils. Biorheology, 28 (6): 557–567. 7

ECK, S., WÖRZ, S., MÜLLER-OTT, K., HAHN, M., BIESDORF, A., SCHOTTA, G., RIPPE, K. and ROHR, K. (2016). A spherical harmonics intensity model for 3d segmentation and 3d shape analysis of heterochromatin foci. Medical image analysis, 32: 18–31. 14

ERDOğAN, S. T. (2016). Simple Estimation of the Surface Area of Irregular 3D Particles. Journal of Materials in Civil Engineering, 28 (8): 04016062. 9

EREMEYEV, V. A., SKRZAT, A., STACHOWICZ, F. and VINAKURAVA, A. (2017). On strength analysis of highly porous materials within the framework of the micropolar elasticity. Procedia Structural Integrity, 5: 446 – 451, 2nd International Conference on Structural Integrity, ICSI 2017, 4-7 September 2017, Funchal, Madeira, Portugal.
URL http://www.sciencedirect.com/science/article/pii/S2452321617303104 1

EVANS, E. and HOCHMUTH, R. (1976). Membrane viscoelasticity. Biophysical Journal, 16 (1): 1–11. 8, 9, 31

EVANS, E. and YEUNG, A. (1989). Apparent viscosity and cortical tension of blood granulocytes determined by micropipet aspiration. Biophysical journal, 56 (1): 151–160. 7

FINLAYSON, B. A. (1972). The Method of Weighted Residuals and Variational Principles. ACADEMIC PRESS, INC. 39

GE, W., MARQUEZ, R., MODEST, M. F. and ROY, S. P. (2015). Implementation of high-order spherical harmonics methods for radiative heat transfer on OpenFOAM. Journal of Heat Transfer, 137 (5): 052701. 18

GORDON-SMITH, T. (2007). Red blood cells. Surgery (Oxford), 25 (2): 57–60. 2

GRAF, M. and POTTS, D. (2009). Sampling sets and Quadrature Formulae on the Rotation Group. Numerical Functional Analysis and optimization, 30 (7–8): 665–688. 16

GRINFELD, P. (2010). Introduction to Tensor Analysis and the Calculus of Moving Surfaces. Springer. 24

GRUTTMANN, F. and TAYLOR, R. L. (1992). Theory and finite element formulation of rubberlike membrane shells using principal stretches. International Journal for Numerical Methods in Engineering, 35 (5): 1111–1126.
URL https://onlinelibrary.wiley.com/doi/abs/10.1002/nme.1620350511 49

GUZAS, E. L. and EARLS, C. J. (2011). Simulating blast effects on steel beam-column members: Methods. Computers & Structures, 89 (23-24): 2133–2148. 11

HAN, D. and CAO, G. (2018). Phase difference between groundwater storage changes and groundwater level fluctuations due to compaction of an aquifer-aquitard system. Journal of Hydrology, 566: 89 – 98. 10

HASKOVEC, J., MASMOUDI, N., SCHMEISER, C. and TAYEB, M. (2011). The Spherical Harmonics Model coupled to the Poisson Equation. Kinetics and Related Models, 4 (4): 1063–1079. 16

HOLZAPFEL, G. A. (2000). Nonlinear Solid Mechanics: A Continuum Approach for Engineering. John Wiley and Sons Ltd. 32, 45

HéNON, S., LENORMAND, G., RICHERT, A. and GALLET, F. (1999). A New Determination of the Shear Modulus of the Human Erythrocyte Membrane Using Optical Tweezers. Biophysical Journal, 76 (2): 1145 – 1151. 7

IBRAHIMBEGOVIć, A. and GRUTTMANN, F. (1993). A consistent finite element formulation of nonlinear membrane shell theory with particular reference to elastic rubberlike material. Finite Elements in Analysis and Design, 13 (1): 75 – 86.
URL http://www.sciencedirect.com/science/article/pii/0168874X9390008E 49

JORDãO, T. and MENEGATTO, V. (2014). Weighted Fourier-Laplace transforms in reproducing kernel Hilbert spaces on the sphere. Journal in Mathematics Analysis and Applications, 411 (2): 732–741. 17

KARAMI, A. and EGHTESAD, M. (2018). Simulation of Active Eye Motion Using Finite Element Modelling. Latin American Journal of Solids and Structures, 15. 1

KENER, J. and POTTS, D. (2008). Fast evaluation of quadrature formulae on the sphere. Mathematics of Computation, 77 (261): 397–419. 16

KIENDL, J., HSU, M.-C., WU, M. C. and REALI, A. (2015). Isogeometric Kirchhoff–Love shell formulations for general hyperelastic materials. Computer Methods in Applied Mechanics and Engineering, 291: 280–303. 29, 49

KOAY, E. J., SHIEH, A. C. and ATHANASIOU, K. A. (2003). Creep indentation of single cells. Journal of biomechanical engineering, 125 (3): 334–341. 7

KOZŁOWSKI, E., KOWALSKA, B., KOWALSKI, D. and MAZURKIEWICZ, D. (2018). Water demand forecasting by trend and harmonic analysis. Archives of Civil and Mechanical Engineering, 18 (1): 140 – 148.
URL http://www.sciencedirect.com/science/article/pii/S1644966517300699
10

KUSHCH, V. I., MOGILEVSKAYA, S. G., STOLARSKI, H. K. and CROUCH, S. L. (2013). Elastic fields and effective moduli of particulate nanocomposites with the Gurtin–Murdoch model of interfaces. International Journal of Solids and Structures, 50 (7-8): 1141–1153. 20

KUTAY, M. E., VARMA, S. and JAMRAH, A. (2017). A micromechanical model to create digital microstructures of asphalt mastics and crumb rubber-modified binders. International Journal of Pavement Engineering, 18 (9): 754–764. 11

LAKES, R. (2009). Viscoelastic Materials. Cambridge University Press. 35

LALANNE, B., ABI CHEBEL, N., VEJRAŽKA, J., TANGUY, S., MASBERNAT, O. and RISSO, F. (2015). Non-linear shape oscillations of rising drops and bubbles: Experiments and simulations. Physics of Fluids, 27 (12): 123305. 21

LALANNE, B., TANGUY, S. and RISSO, F. (2013). Effect of rising motion on the damped shape oscillations of drops and bubbles. Physics of Fluids, 25 (11): 112107. 21

LEWEKE, S., MICHEL, V. and SCHNEIDER, N. (2018). Vectorial Slepian Functions on the Ball. Numerical Functional Analysis and Optimization, 39 (11): 1120–1152. 17

LIM, C., DAO, M., SURESH, S., SOW, C. and CHEW, K. (2004). Large deformation of living cells using laser traps. Acta Materialia, 52 (7): 1837 – 1845. 7

LIM, C., ZHOU, E. and QUEK, S. (2006). Mechanical models for living cells—a review. Journal of Biomechanics, 39 (2): 195 – 216. 6, 7

LIU, Y.-Y., TENG, B., CONG, P.-W., LIU, C.-F. and GOU, Y. (2012). Analytical study of wave diffraction and radiation by a submerged sphere in infinite water depth. Ocean Engineering, 51: 129–141. 11

MENEGATTO, V. and PIANTELLA, A. (2011). Old and new on the Laplace-Beltrami derivative. Numerical Functional Analysis and Optimization, 32 (3): 309–341. 16

MEYERS, M. A., CHEN, P.-Y., LIN, A. Y.-M. and SEKI, Y. (2008). Biological materials: Structure and mechanical properties. Progress in Materials Science, 53 (1): 1 – 206.
URL http://www.sciencedirect.com/science/article/pii/S0079642507000254
3

MIJAILOVICH, S. M., KOJIC, M., ZIVKOVIC, M., FABRY, B. and FREDBERG, J. J. (2002). A finite element model of cell deformation during magnetic bead twisting. Journal of Applied Physiology, 93 (4): 1429–1436. 7

MILLS, J., QIE, L., DAO, M., LIM, C., SURESH, S. and OTHERS (2004). Nonlinear elastic and viscoelastic deformation of the human red blood cell with optical tweezers. MCB-TECH SCIENCE PRESS-, 1: 169–180. 7

MODEST, M. F., CAI, J., GE, W. and LEE, E. (2014). Elliptic formulation of the simplified spherical harmonics method in radiative heat transfer. International Journal of Heat and Mass Transfer, 76: 459–466. 18

MOITA, G. F. (1994). Non-linear finite element analysis of continua with emphasis on hyperelasticity. Ph.D. thesis, Imperial College London. 49

MONS, V., CAMBON, C. and SAGAUT, P. (2016). A spectral model for homogeneous shear-driven anisotropic turbulence in terms of spherically averaged descriptors. Journal of Fluid Mechanics, 788: 147–182. 20

MOONEY, M. (1940). A Theory of Large Elastic Deformation. Journal of Applied Physics, 11 (9): 582–592.
URL https://doi.org/10.1063/1.1712836 8, 34

NEEDLEMAN, A. (1977). Inflation of spherical rubber balloons. International Journal of Solids and Structures, 13 (5): 409 – 421.
URL http://www.sciencedirect.com/science/article/pii/0020768377900361 49

NIORDSON, F. I. (1985). Shell Theory. ELSEVIER SCIENCE PUBLISHERS B.V. 6, 23, 25

PAL, G. and MODEST, M. F. (2015). Advanced differential approximation formulation of the PN method for radiative transfer. Journal of Heat Transfer, 137 (7): 072701. 18

PENG, Z., ASARO, R. J. and ZHU, Q. (2011). Multiscale modelling of erythrocytes in Stokes flow. Journal of Fluid Mechanics, 686: 299–337. 8

POTTS, D., PRESTIN, J. and VOLLRATH, A. (2009). fast algorithm for nonequispaced Fourier transforms on the rotation group. Numerical Algorithms, 52 (3): 355–384. 16

POTTS, D., STEIDL, G. and TASCHE, M. (1998). Fast and stable algorithms for discrete spherical Fourier transforms. Linear Algebra and its Applications, 276: 433–450. 16

POZRIKIDIS, C. (1992). Boundary Integral and Singularity Methods for Linearized Viscous Flow. Cambridge Texts in Applied Mathematics. Cambridge University Press. 51

POZRIKIDIS, C. (2005). Axisymmetric motion of a file of red blood cells through capillaries. Physics of Fluids, 17 (3): 031503.
URL https://doi.org/10.1063/1.1830484 51, 53

RAND, R. and BURTON, A. (1964). Mechanical Properties of the Red Cell Membrane: I. Membrane Stiffness and Intracellular Pressure. Biophysical Journal, 4 (2): 115 – 135. 6

RIVLIN, R. S. and RIDEAL, E. K. (1948). Large elastic deformations of isotropic materials IV. further developments of the general theory. Philosophical Transactions of the Royal Society of London. Series A, Mathematical and Physical Sciences, 241 (835): 379–397. 8, 34

ROSS, M. and PAWLINA, W. (2011). Histology: a text and atlas: with correlated cell and molecular biology. Vol. 6. Lippincott Williams Wilkins. 2

SANKAR, M. and MAZUMDER, S. (2012). Solution of the Radiative Transfer Equation in Three-Dimensional Participating Media Using a Hybrid Discrete Ordinates: Spherical Harmonics Method. Journal of Heat Transfer, 134 (11): 112702. 18

SARKAR, D., OSBORNE, M. A. and ADCOCK, T. A. (2018). Prediction of tidal currents using Bayesian machine learning. Ocean Engineering, 158: 221 – 231. 10

SATCHER, R. and DEWEY, C. F. (1996). Theoretical estimates of mechanical properties of the endothelial cell cytoskeleton. Biophysical journal, 71 (1): 109–118. 7

SATO, M., THERET, D., WHEELER, L., OHSHIMA, N. and NEREM, R. (1990). Application of the micropipette technique to the measurement of cultured porcine aortic endothelial cell viscoelastic properties. Journal of biomechanical engineering, 112 (3): 263–268. 7

SCHMID-SCHÖNBEIN, G., SUNG, K.-L., TÖZEREN, H., SKALAK, R. and CHIEN, S. (1981). Passive mechanical properties of human leukocytes. Biophysical Journal, 36 (1): 243–256. 7

SHEN, J., TANG, T. and WANG, L.-L. (2011). Spectral methods: algorithms, analysis and applications. Vol. 41. Springer Science & Business Media. 38

SKALAK, R., TOZEREN, A., ZARDA, R. and CHIEN, S. (1973). Strain Energy Function of Red Blood Cell Membranes. Biophysical Journal, 13 (3): 245 – 264.
URL http://www.sciencedirect.com/science/article/pii/S0006349573859831
31

SOLEIMANI, M., SAHRAEE, S. and WRIGGERS, P. (2018). Red blood cell simulation using a coupled shell-fluid analysis purely based on the SPH method. Biomechanics and Modeling in Mechanobiology, .
URL https://doi.org/10.1007/s10237-018-1085-9 8

SWARZTRAUBER, P. (2003). On Computing the Points and Weights for Gauss–Legendre Quadrature. SIAM Journal on Scientific Computing, 24 (3): 945–954.
URL https://doi.org/10.1137/S1064827500379690 41

SWARZTRAUBER, P. N. (1993). The vector harmonic transform method for solving partial differential equations in spherical geometry. Monthly Weather Review, 121 (12): 3415–3437. 3

SWARZTRAUBER, P. N. and SPOTZ, W. F. (2000). Generalized discrete spherical harmonic transforms. Journal of Computational Physics, 159 (2): 213–230. 39

TANG, Y.-H., LU, L., LI, H., EVANGELINOS, C., GRINBERG, L., SACHDEVA, V. and KARNIADAKIS, G. E. (2017). OpenRBC: A Fast Simulator of Red Blood Cells at Protein Resolution. Biophysical Journal, 112 (10): 2030 – 2037.
URL http://www.sciencedirect.com/science/article/pii/S0006349517304368
9

TUTAR, I. B., PATHAK, S. D., GONG, L., CHO, P. S., WALLNER, K. and KIM, Y. (2006). Semiautomatic 3-D prostate segmentation from TRUS images using spherical harmonics. IEEE transactions on medical imaging, 25 (12): 1645–1654. 13

WANG, Y. and DIMITRAKOPOULOS, P. (2006). A three-dimensional spectral boundary element algorithm for interfacial dynamics in Stokes flow. Physics of Fluids, 18 (8): 082106. 38

WRIGGERS, P. and TAYLOR, R. (1990). Fully non-linear axisymmetrical membrane element for rubber-like materials. Engineering Computations, 7: 303–310. 49

XU, H. and PATTERSON, M. S. (2006). Application of the modified spherical harmonics method to some problems in biomedical optics. Physics in Medicine & Biology, 51 (12): N247. 13

YANG, D., WANG, L., CHEN, D., YAN, C., HE, X., LIANG, J. and CHEN, X. (2018). Filtered maximum likelihood expectation maximization based global reconstruction for bioluminescence tomography. Medical & biological engineering & computing, 56 (11): 2067–2081. 15

YAZDANI, A. and BAGCHI, P. (2013). Influence of membrane viscosity on capsule dynamics in shear flow. Journal of Fluid Mechanics, 718: 569–595. 9, 36

YOON, D. and YOU, D. (2016). Continuum modeling of deformation and aggregation of red blood cells. Journal of Biomechanics, 49 (11): 2267 – 2279, selected Articles from the International Conference on CFD in Medicine and Biology (Albufeira, Portugal – August 30th - September 4th, 2015).
URL http://www.sciencedirect.com/science/article/pii/S0021929015006697
8

Annex I

Surface properties: Sphere

Coordinates transformation

$$x(\theta,\phi) = R\sin\theta\cos\phi,\ y(\theta,\phi) = R\sin\theta\sin\phi,\ z(\theta,\phi) = R\cos\theta \tag{I.1}$$

Cartesian metric tensor

$$Z_{ij} = \begin{bmatrix} 1 & 0 & 0 \\ 0 & 1 & 0 \\ 0 & 0 & 1 \end{bmatrix} \tag{I.2}$$

Shift tensor

$$Z^i_\alpha = \begin{bmatrix} R\cos\theta\cos\phi & -R\sin\theta\sin\phi \\ R\cos\theta\sin\phi & R\sin\theta\cos\phi \\ -R\sin\theta & 0 \end{bmatrix} \tag{I.3}$$

metric tensor

$$a_{\alpha\beta} = \begin{bmatrix} R\cos\theta\cos\phi & R\cos\theta\sin\phi & -R\sin\theta \\ -R\sin\theta\sin\phi & R\sin\theta\cos\phi & 0 \end{bmatrix} \begin{bmatrix} R\cos\theta\cos\phi & -R\sin\theta\sin\phi \\ R\cos\theta\sin\phi & R\sin\theta\cos\phi \\ -R\sin\theta & 0 \end{bmatrix} = \begin{bmatrix} R^2 & 0 \\ 0 & R^2\sin^2\theta \end{bmatrix} \tag{I.4}$$

normal vector $\mathbf{n}$

$$\mathbf{n} = \frac{\frac{dx}{d\theta}}{||\frac{dx}{d\theta}||} = \begin{vmatrix} \mathbf{i} & \mathbf{j} & \mathbf{k} \\ R\cos\theta\cos\phi & R\cos\theta\sin\theta & -R\sin\theta \\ -R\sin\theta\sin\phi & R\sin\theta\cos\phi & 0 \end{vmatrix} = \begin{pmatrix} R^2\sin^2\theta\cos\phi \\ R^2\sin^2\theta\sin^2\phi \\ R^2\sin\theta\cos\theta \end{pmatrix} = \begin{pmatrix} \sin\theta\cos\theta \\ \sin\phi\cos\phi \\ \cos\theta \end{pmatrix} \tag{I.5}$$

covariant derivative of the normal vector

$$\nabla_\alpha N^i = \frac{\partial N^i}{\partial S^\alpha} = \begin{bmatrix} \cos\theta\cos\phi & -\sin\theta\sin\phi \\ \cos\theta\sin\theta & \sin\theta\cos\phi \\ -\sin\theta & 0 \end{bmatrix} \tag{I.6}$$

curvature tensor

$$b_{\alpha\beta} = -Z^i_\alpha \nabla_\beta N^i = -\begin{bmatrix} R & 0 \\ 0 & R\sin^2\theta \end{bmatrix} \tag{I.7}$$